Surface Structure of Single-Crystal Hexagonal Ice

A senior honors thesis for the Department of Chemistry

Alexandra Brumberg

Tufts University, 2016

TABLE OF CONTENTS

TABLE OF FIGURES

1 INTRODUCTION

Single-crystal surfaces give surface scientists the ability to study the properties of specific arrangements of atoms and, in particular, the reactivity of each of the crystalline faces. Perhaps the best example of this comes from studies done on the faces of body-centered cubic single-crystal iron to reveal that the (111) face is over 16 times more reactive than the (100) or (110) faces.[1] This insight allowed industrial chemists to maximize the production of ammonia fertilizer in the Haber-Bosch process, which further enabled the exponential increase in Earth's sustainable human population that had begun with the introduction of the process decades earlier.[2] Although such insights are overwhelmingly common in metal surface studies, for ice—one of the most fundamental hydrogen-bonding surfaces, relevant in contexts from cells and clouds to interstellar space—very little is known.

Ice provides an enticing system to study due to its regular structure and minimized molecular motion compared to water. Although hydrogen bonding imparts intriguing properties onto water, it also complicates the analysis in ways such as spectral peak broadening. The motion of the hydrogen bonds ultimately makes it very difficult to gain an accurate picture of water's behavior. In ice, the hydrogen-bonding network is partially immobilized due to the lower temperature, thus reducing the magnitude of the complications that occur with water and making experimental studies feasible.

The limiting step to performing surface studies on ice is the inability to produce desired ice faces. While it is straightforward to manufacture a given crystallographic face of a metal, there is no well-established method for generating a specific face of ice. In fact, there are few research groups in the world even capable of growing single-crystal ice to begin with. The ease with which a specific surface of a metal can be prepared has yet to be attained for the production of ice.

Ultimately, growing single-crystal ice for experiments comes down to growing high-quality ice efficiently. Although ice may appear to be single-crystal with certain characterization techniques, spectroscopy is less forgiving—the fewer the defects, the better a spectrum will render. Since spectroscopy is one of the most powerful tools for studying reactions at surfaces, the ability to produce high-quality single-crystal ice is of the utmost importance. Natural single-crystal ice that forms in glaciers is not used in spectroscopic studies precisely because its dislocation density is too high (in addition to its being difficult to obtain and there being no way to control its orientation).[3]

A natural place to begin for single-crystal ice growth is with the prominent single-crystal metal growth techniques, and indeed a number of prominent metal growth techniques have been applied to single-crystal ice growth. In the Bridgman technique, growth is initiated with a polycrystalline seed that is then melted away until only a single crystal remains; that single crystal is then used to seed growth as the crucible is lowered through a bath with a temperature gradient.[4] The Stockbarger modification of the Bridgman technique employs two baths that allow for better temperature control of the gradient, and thus result in better single-crystal growth.[5] The Czochralski method (most notable for its production of single-crystal

silicon and semiconductor ingots for electronics) also uses a seed crystal. The seed is mounted on a rod or placed in a capillary and then inserted into the melt (i.e. liquid) of the pure material, after which it is raised out of the bath under controlled conditions.[6] Both the Bridgman and Czochralski methods provide the advantage of producing single crystals of a specific crystallographic orientation due to the use of the seed crystal;[7] the inability of the modified Bridgman technique to do so is a major disadvantage.

Both of these methods have been used to grow ice with varying degrees of success. When ice grown with the Bridgman method is compared to ice grown with the Czochralski method, it is of higher quality (lower defect density) and grown at a faster rate.[3] The effect is significant, as the Czochralski method requires a slow growth rate of 1 mm/day in order to obtain the same low dislocation density of the Bridgman technique (maintained up to a growth rate of 8.64 mm/day).[3] The rate of crystal growth is a major consideration, as a faster growth rate allows more ice to be produced in a shorter time frame. It is not practical to work with ice that needs to be grown at 1 mm/day; to put this number in context, each experiment in the Shultz lab requires a sample that is 1 cm thick.

Other techniques have also been employed for growing single-crystal ice, with practically as many techniques available today as there are groups researching ice. One example is the Knight technique, in which a large tub is cooled until the top layer freezes over, and then proceeds downward as it would in a freezing lake.[8] In a similar technique, water is cooled specifically using a vacuum system; the top layer of water is the first to freeze, and then once again growth progresses downward.[9] There is also the zone-refining technique, which uses natural convection to create homogenous crystals.[10] Evidently, there are a wide variety of growth methods available, and the choice depends on what suits the needs of the experiment.

The method that the Shultz lab has developed is based off of the modified Bridgman-Stockbarger technique.[5,11] In 2013, the Shultz group successfully refined their growth technique to produce single-crystal ice reliably.[12,13] This work had been the culmination of three graduate students' efforts to adapt the Bridgman growth technique to growing large samples of single-crystal ice.[12,14,15] However, apart from sum frequency generation (SFG) spectroscopy, very little characterization had been done to analyze the products of this ice growth technique, as the focus had been on obtaining a spectrum of the ice surface.

Over the course of the last three years, we have further refined the growth technique and worked to characterize the ice that results from its growth. This thesis covers a wide range of projects concerning single-crystal ice that collectively enable a greater understanding of the surface structure and chemistry of ice. The Shultz lab now has the ability to work with any crystallographic face of ice, meaning that studies can be done on the basal, primary prism, or secondary prism faces—a crucial step in being able to piece together the chemistry of these surfaces.[16]

2 THEORY

The difficulty in growing large, high-quality single-crystal ice is not unfounded. This theory section provides an overview of the challenges associated with growing single-crystal ice and the properties that need to be taken into consideration. The theory section begins with a discussion of the properties of ice, followed by how those properties change when H_2O is replaced by D_2O. The section concludes with a brief introduction to differential interference contrast microscopy, an imaging tool that we propose to use to investigate the surface of ice.

2.1 PROPERTIES OF ICE

For all solids, there is some inherent difficulty in growing large, high-quality single crystals. The material must be cooled to below its freezing temperature and have a nucleation site upon which crystals can form, requirements which present a special challenge for ice. The particular challenges are discussed below and presented with the solutions that have been developed. Each ice single-crystal growth technique addresses these concerns in its own way, ultimately impacting the properties of the resulting ice. Once growth begins, the interfacial energies of all of the crystallographic faces control the growth rate of each face in a given direction. It is these energies that define the hexagonal crystal structure of ice grown at atmospheric pressure and 0 °C.

2.1.1 Structure of Hexagonal Ice

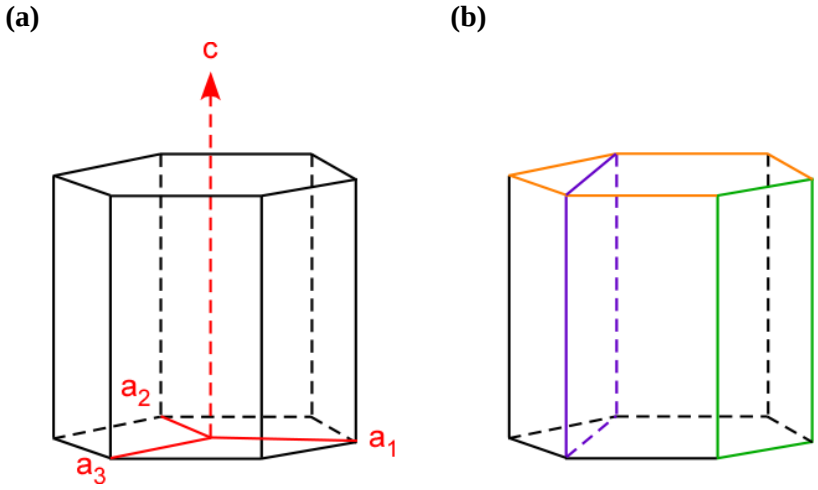

Figure 1. The hexagonal structure of ice I_h. (a) Location of the three *a*-axes and the *c*-axis. (b) The basal face (**orange**), primary prism face (**green**), and secondary prism face (**purple**).

Hexagonal ice I_h has a hexagonal crystal structure, as shown in Figure 1. The crystal structure is defined by two main axes. The *a*-axis is parallel to the hexagonal base; the a_1, a_2, and a_3 axes are 120° apart and each run from the center of the hexagon to one of the corners. The *c*-axis is perpendicular to the three *a*-axes.

These axes can be used to define the three faces of the hexagonal lattice: basal, primary prism, and secondary prism. The basal face is the hexagonal face of the hexagonal prism and is perpendicular to the *c*-

axis. The primary prism face is the rectangular face of the hexagonal prism, parallel to the *a*-axis. The secondary prism face, in turn, is perpendicular to the *a*-axis. The *a*-axis that is considered does not affect the identity of a face.

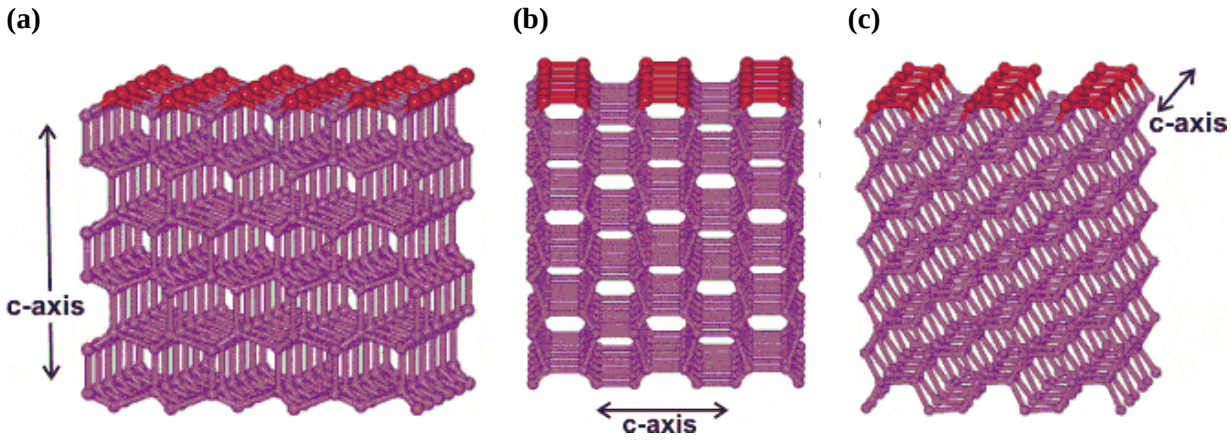

Figure 2. Molecular representation of the three main faces of ice I_h. The atoms and bonds highlighted in red are those that are at the surface. (a) is the basal face, while (b) and (c) are typically represented as the primary prism and secondary prism faces, respectively. (Images taken from Ref. 17).

Although the definitions of the three faces are agreed upon, the difficulty lies in figuring out *which* hexagon defines these three faces and thus where the *a*-axis is located. The hexagon formed by the basal face of atoms is different than the hexagon formed by the hexagonal close-packed (hcp) unit cell used by crystallographers. The molecular image of the primary and secondary prism faces (Figure 2) is swapped in the two scenarios, and the interpretation of spectra changes depending on which is used. An experiment has been proposed to resolve this dilemma, the results of which are currently being interpreted. This thesis will use the molecular model, in which the hexagon is taken to be the molecular hexagon formed by the atoms themselves and visibly apparent when looking at a model. This is in line with the previous work that has been done by the group; furthermore, interpretation of etch pits does not change depending on whether the molecular or crystallographic method is used in the definition.

The surface energies of each of these faces are very similar.[18] For the ice-water interface, the interfacial energies of the basal, primary prism, and secondary prism faces were theoretically calculated to be 23.3, 23.6, and 24.7 mJ m^{-2}, respectively, by using the TIP4P model of water.[19] Although their results are 20% off from experimental estimates (evidence of the challenges that afflict theoretical models of water), they effectively demonstrate how close the values are. As such, it is difficult to determine which is the most stable, particularly under a specific set of conditions since there is a strong sensitivity to the temperature.[18,20] (This is what causes the variation in the shape of a snowflake.[*]) The question of which face is the most stable is an active area of research, but a difficult one to answer since experiments are critically sensitive to

[*] In fact, it was recently shown that if two snowflakes are grown under precisely the same conditions, identical snowflakes can be produced.[43] The saying, "No two snowflakes are alike," is really just a demonstration of the strong sensitivity of the interfacial energies to growth conditions.

the conditions used. A major focus of my work has involved investigating the energies of the different faces in relation to one another and to the other crystallographic faces as well.

Furthermore, both the structure and the properties of ice are dependent upon the ice nucleation source. One counterintuitive example showed that ice grown on a BaF_2 substrate is hydrophobic.[21] It is for this reason that growing ice from the melt without a foreign nucleation source is necessary; it is the only way to gain insight into the natural properties of ice.

2.1.2 Thermodynamic Growth

Though growing single-crystal ice from the melt may seem to be straightforward, in reality it presents a number of complications. The primary issue is that pure water has the tendency to supercool; that is, it can be cooled to significantly below 0 °C (as low as –38 °C) before it begins to freeze.[22] When the ice finally begins to grow, its growth is a kinetic process.[23] In these circumstances, ice growth is governed by kinetics, rather than by thermodynamics: the properties of the ice—including the most favored growth face—are determined by what is most kinetically stable. In order to study thermodynamic ice properties, the ice must be growth under thermodynamic conditions.

To avoid the issue of supercooling and the ensuing kinetic growth, ice growth is initiated with a polycrystalline seed that is created by cooling the tip of the crucible below –38 °C (see Section 3.1.2). The crucible has a special design that enables the numerous domains present in the polycrystalline seed to be competitively eliminated as growth proceeds through the crucible capillary. The most stable face has a larger and larger area at the interface as growth progresses, so that the less stable faces have a smaller and smaller area until they are completely eliminated. Typically this selection occurs entirely within the capillary, such that the bulb of the crucible only has one domain; however, on the occasions when multiple domains survive the bulb, the neck of the crucible is typically successful in eliminating the least stable domains (those where the advancing front has a high interfacial energy). The ice that then grows through the remainder of the crucible is single-crystal and grows with the most stable face exposed at the surface.

The kinetic sampling of faces in the polycrystalline seed means that we are unable to intentionally reproduce a given sample orientation. The face that is exposed at the ice-water interface is arbitrary in the sense that it is determined by which face is the most thermodynamically stable of the ones that are produced in the polycrystalline seed. However, *the* most thermodynamically stable face of ice I_h for the ice-water interface is not necessarily seen; if it were, there would unfortunately be no method of even identifying it as such. It is also not possible to eliminate any other determinant factors in the growth process that could account for the variability of face selection.

2.1.3 Wulff Construction

In the late 19th century, Curie published a paper illustrating how surface energies could be used to determine the ratio of the areas of faces of a rectangular prismatic crystal.[24] Wulff later elaborated on this concept by postulating that it could be done for any crystal, so long as the surface energies of each of the faces were known;[25] the correct proof of this was provided later that year by von Laue.[26] This theory (deemed the Wulff

construction) has been widely applied to crystal and nanoparticle growth, as it directly demonstrates how the shape of a crystal is related to a thermodynamic property: surface energy.

The natural question that arises is whether or not the theory of the Wulff construction can be applied to ice in the reverse: knowing the ratio of the areas of the basal face to the primary prism face, can the surface energies be determined? Since etching (described in Section 3.2.4) yields an etch pit whose sides correspond to the basal and primary prism faces, perhaps it is possible to measure the areas of the faces to determine their surface energies.

Unfortunately, complications arise that make the idea of using etch pit geometry to calculate surface energy too difficult or even impossible. Beyond the geometric complexity that arises from using a hexagonal prism to create etch pit shape, there is also a concern regarding whether the answer truly gives the surface energies of the faces at the ice-air interface, considering that there is a layer of the etch polymer between the two. The mere presence of the solvent in which the polymer is dissolved also prevents the existence of a true ice-air equilibrium, and so the application of the Wulff construction to the ice etch pits would not yield accurate results.

This issue has also been treated by Libbrecht in the first paper of his series of articles reviewing the state of ice research.[27] He addresses the same issue of the lack of known values for the interfacial energies at the ice-vapor interface. Neither experiment nor theory has been successful in advancing the topic, partially because of the lack of understanding of the behavior of the ice surface (for example, with regards to surface melting and reconstruction). He also mentions that the equilibration times for even small crystals is very long (e.g. greater than a week for a 1 mm crystal), especially when there are background gases in the air (as there are in our freezer), such that it places significant doubt on whether we are working with crystals in equilibrium at all.

2.2 D_2O Ice

The single-crystal growth procedure for ice has been so extensively studied and perfected in the Shultz lab because of its initial application to sum frequency generation (SFG) experiments. However, the question arises of how the apparatus and procedure for single-crystal ice growth can be modified for other growth types. For example, can deuterated (D_2O) ice be grown under similar laboratory conditions? The ability to grow such ice would be useful for isotopic studies with SFG, in which the identification of a peak could be verified by substituting each hydrogen on water with deuterium and watching the peak shift that results. Though the addition of a neutron to each hydrogen in the water molecule may seem innocuous, it has a drastic effect on the properties of D_2O and ultimately causes a number of changes to the thermodynamic properties that are involved in the freezing process.

Firstly, the freezing point of D_2O at atmospheric pressure is 3.82 °C, roughly four degrees higher than that of H_2O.[28] Gibbs' Law of Free Energy for a phase transition ($\Delta G = 0$) yields the following relationship:

$$\Delta S = \frac{\Delta H}{T}$$

The heat of fusion for D_2O is also higher, at 6.305 kJ/mol, compared to that of 6.008 kJ/mol for H_2O.[28] The change in entropy, however, is roughly the same—the difference in the number of microstates available for D_2O ice compared to H_2O ice is minimal—thus T must be higher since ΔH is higher. Additionally, since the strength of the D_2O hydrogen bond is higher,[29] the increase in hydrogen bond strength results in a greater intermolecular attraction between water molecules and thus a higher melting point (and higher freezing point).

Because the heat of fusion for D_2O is higher, the heat of solidification will be greater in magnitude (more negative). Thus D_2O releases more heat as it freezes; this heat needs to be dissipated by the system its surroundings. During ice growth, heat is dissipated through the ice beneath it, the water above it, and out of the crucible into the ethylene glycol bath (see Section 3.1.1 for a description of the growth chamber). It is therefore important to maintain a considerable amount of water above the final ice front, not only to dissipate heat, but also to prevent low-purity ice from forming. As ice grows, it expels impurities such as dissolved gases. If all of the available water were used, then the final layers of ice would either not be single-crystal or contain a higher defect density due to impurities present in the water used to grow that portion of ice.

There is also the issue of thermal conductivity. As mentioned above, as ice grows, the heat of solidification must be dispersed throughout the system. Ice, in general, has a higher thermal conductivity than does water, so the ice beneath the ice-water growth front is critical in dissipating the heat that is produced during ice growth. The liquid thermal conductivity of D_2O at 3.82 °C is higher than that of H_2O at 0 °C, at 0.565 W m^{-1} K^{-1} versus 0.5562 W m^{-1} K^{-1}, respectively.[30,31] How this will effect ice growth cannot be made immediately clear, as D_2O has both a higher heat of solidification and a higher thermal conductivity. Nevertheless, thermal conductivity is one of the major factors that influences the shelf temperature. If the shelf temperature were too warm (e.g. exactly at 0 °C for H_2O, or 3.82 °C for D_2O), then as ice would grow, it would melt the most recently-grown layer of ice beneath it.

Collectively, these different properties for D_2O indicate that modification of the ice growth procedure for D_2O should not be as straightforward as simply raising all of the temperatures involved by 3.82 °C. The thermodynamic differences between D_2O and H_2O will affect its environment when it freezes; by studying the differences between D_2O and H_2O ice growth, it is possible to gain insight into the thermodynamic properties of water.

2.3 Differential Interference Contrast Microscopy

Differential interference contrast microscopy (DIM) is an imaging technique that utilizes optical interferometry to enhance the contrast of an image.[32–34] Through the use of interferometry, it is capable of measuring changes in surface topology or surface composition (i.e. refractive index), because both changes result in an optical path difference.

In DIM, a laser passes through a Nomarski prism and is thereby separated into two beams of equal amplitude. These two beams can either be transmitted through or reflected off of the sample, after which they are recombined by either another or the same Nomarski prism. If they experienced an optical path length difference, either due to a difference in the distance traveled (due to surface morphology) or due to different refractive indices in the parts of the sample they traveled through, then there is a phase difference between the two beams. This phase difference manifests as either constructive or destructive interference; when the beam reaches the detector, the relative intensity of the beam will create a map of the surface based on this information.

2.3.1 Nomarski Prism

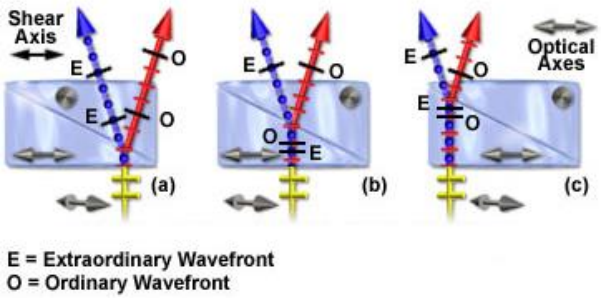

Figure 3. Separation of ordinary and extraordinary components of a beam passing through a Wollaston prism. (Image taken from Ref. 34.)

A Nomarski prism is, at its core, simply a beam splitter. It is made of two wedges of optical quartz that are glued together. Quartz is a birefringent material, meaning that its refractive index varies depending on the polarization of the light that traveling through it and the direction of travel. Light that is polarized perpendicular to the optical axis is called the ordinary wave and travels along the fast axis of a Nomarski prism (i.e. the axis with the lower index of refraction); conversely, light that is polarized parallel to the optical axis is called the extraordinary wave and travels along the slow axis of the prism (i.e. the axis with the higher index of refraction).

The Nomarski prism is a special case of a Wollaston prism (Figure 3). In a Wollaston prism, the optical axes of the two pieces of quartz are orthogonal to one another. When the beam enters the prism, nothing happens; upon crossing into the second piece of quartz, the beam is split into its ordinary and extraordinary components. The beams diverge and continue to do so upon exiting the prism. The distance between the beams is called the shear and depends on where the beam enters the prism.

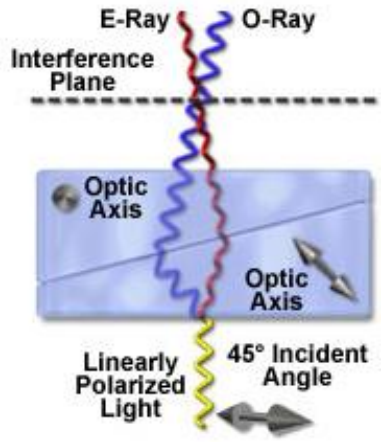

Figure 4. Separation of ordinary and extraordinary components of a beam passing through a Nomarski prism. (Image taken from Ref. 34.)

In a Nomarksi prism (Figure 4), one of the optical axes is oblique at a 45° angle. Light enters into the wedge with the oblique optical axis, and as a result of this, the ordinary and extraordinary rays immediately separate, because the ordinary ray will travel along the fast axis while the extraordinary ray travels along the slow axis. Upon crossing into the second wedge, they are refracted such that they cross paths. In particular, the location at which they cross paths—called the interference plane—is outside of the prism. This makes the Nomarski prism easier to use, as the position of the interference plane and the splitting angle (the angle at which they cross) can be more easily controlled and visualized.

3 EXPERIMENTAL

3.1 SINGLE-CRYSTAL GROWTH PROCEDURE

The use of a modified Bridgman apparatus with a crucible to grow single crystals has long been established.[35] Though the use of such a technique for growing ice crystals is unusual (although not unprecedented), its success is not surprising in that metal crystals have been grown in such a way for decades.[4]

3.1.1 Modified Bridgman Apparatus

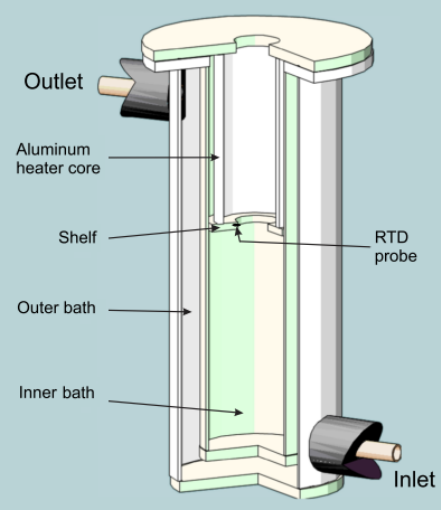

Figure 5. A cut-away of the modified Bridgman apparatus. The crucible progresses downward through the machine; growth occurs at the shelf. (Image taken from Ref. 11.)

A modified Bridgman-Stockbarger apparatus[5] is used to grow ice.[11] The apparatus is regulated by a motor that controls the vertical movement of the crucible. The middle of the machine contains a shelf whose temperature is controlled by a computer. When the crucible passes through the shelf, ice growth occurs. The step size and rate of the motor are controlled by the same computer (see Section 3.1.5) to ensure single-crystal growth; having either parameter be too large would not result in single-crystal ice.

The machine rests on an optical granite table that floats on three columns of nitrogen. The flow of nitrogen is maintained by an ultra-high pressure gas cylinder whose pressure output is regulated to release 30 psi. This arrangement minimizes vibrations, ensuring that the descent of the crucible through the machine is steady and stable. Excess vibrations would result in polycrystalline ice.

Within the apparatus is an outer bath of ethylene glycol and water maintained at –3 °C; the temperature is set by a chiller that is connected to the outer bath via piping. Ethylene glycol is used primarily for its high thermal conductivity. There is an inner bath filled with 100% ethylene glycol; in addition to being thermally conductive, ethylene glycol is highly viscous and thus minimizes flow within the bath. This establishes a temperature gradient in the vertical (but not horizontal) direction, precisely what is needed for layer-by-layer ice growth.

The chiller that controls the outer bath temperature is connected via tubing that allows for the bath to be pumped continuously. The chiller contains ethylene glycol, which gradually takes in water from the atmosphere since ethylene glycol is hygroscopic. In order to maintain proper ice growth conditions in the outer bath, the ratio of ethylene glycol to water in the chiller should be kept around 70%; lower percentages produce boules in which secondary domains are seen along the walls of the crucible. Additionally, the set point of the chiller needed to establish –3 °C in the outer bath depends upon the ethylene glycol ratio. At 70%, it has ranged from –2.65 °C to –2.55 °C.

The percentage of ethylene glycol in the chiller bath is determined by extracting about 400 mL from the bath and placing it in a tall graduated cylinder; after the liquid warms to room temperature, the specific gravity is measured using a hydrometer. The ice growth machine has a LabVIEW program that uses the specific gravity and temperature to identify the weight percentage of ethylene glycol.

The temperature within the inner bath is not controlled directly, and in fact there is a temperature gradient that is established due to the difference between the temperature at the top and the bottom. The bottom of the inner bath is roughly –3 °C and controlled primarily by the temperature of the outer bath. On the other hand, the top of the bath is roughly 3 °C because it is exposed to the atmosphere; the room temperature thus influences the bath temperature. This establishes a temperature gradient at the shelf that is steep enough to promote ice growth, but not so steep that the necessary high temperature at the top of the bath causes excessive vaporization.

3.1.2 Crucible Design

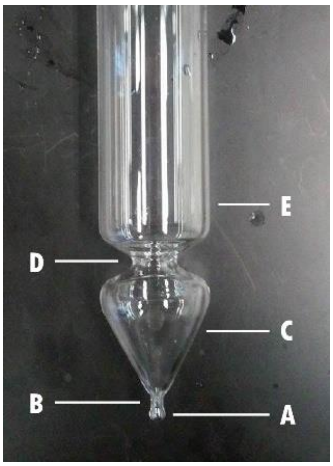

Figure 6. Crucible shape.

As previously discussed, one of the difficulties in growing single-crystal ice is that water supercools. One way to avoid supercooling is to provide a nucleation site, the best option being ice itself so that the resulting ice does not have properties that are influenced by the substrate.

This is done by implementing a competitive growth scheme, in which a polycrystalline seed is prepared by shock-freezing the water in the small bubble (A) at the end of our custom-designed crucible. The first inch of growth in the area of the bulb (B, C) is polycrystalline in the sense that there are multiple single-crystal domains. As the bulb narrows (C), the less energetically stable faces are eliminated. By the time the ice reaches the neck of the crucible (D), only one single-crystal face remains—and it is that of the most energetically stable face.

On occasion, two single-crystal domains share a vertical domain wall. The domains begin in the bulb and survive the neck due to the positioning of the domain wall. There are also occasions on which a much smaller, secondary single-crystal domain is present. In these cases, the secondary is typically eliminated by the wall of the crucible as growth progresses.

The crucible is 1 inch in diameter and 16 inches in length. A piece of tape is wrapped around the crucible so that a line can be drawn marking 14 inches from the bottom. The 14-inch mark is used when mounting the crucible in the machine; the shelf is located 14 inches from the top of the mounting box, and so this arrangement ensures that the tip of the crucible is at the top of the shelf when ice growth begins. Because of the size of the machine, the largest boule that can be grown is roughly 6 inches in length, of which 2 inches are located within the bulb and thus are lost when the boule is extracted from the crucible. The diameters of the boules vary depending on how much ice melts during the extraction process.

3.1.3 Purification and Preparation

Before a sample can be grown, the crucible must be properly washed and care must be taken to purify the water as much as possible to avoid contamination. The preparation begins with an acid "wash," in which the crucible is filled with concentrated sulfuric acid/NOCHROMIX® for at least a day. Following the acid bath are three water baths: the crucible, after being in an acid bath for at least a day, is rinsed with ultrapure water (18.20 MΩ, UV-irradiated water) five times, and then filled entirely. The crucible is never dried completely and always remains filled with water when it is not being used to grow ice. Over the course of the preparation, two more rinses are performed, in which the crucible is rinsed three times with the ultrapure water, before being filled to the top once more with water. If the crucible has been sitting for a long time with the same water, an additional water bath should be given a few days prior to ice growth.

Figure 7. Vacuum line used for degassing.

Preparation the day of ice growth begins with emptying the crucible and filling it with 7 inches of ultrapure water. The crucible is covered with Teflon tape, which is secured using an o-ring. To attach the crucible to the vacuum line, a small slit is cut in the Teflon tape and a piece of glass tubing (attached to the Tygon tubing of the vacuum line) in a septum cap is used to seal the connection between the crucible and the vacuum line.

The water then undergoes degassing for two hours on the vacuum line pictured in Figure 7. Degassing ensures that any dissolved gases are removed before ice growth. The crucible is placed in a Dewar filled with an ice water bath to pre-chill the water in the crucible to 0 °C. The vacuum line is brought to roughly 22 torr by slightly opening the needle valve to the atmosphere. This pressure ensures that the sample is degassed, but without any loss of water, as the vapor pressure of water at room temperature is about 20 torr.

After degassing, the crucible is pre-chilled in the ice-growing machine until the shelf temperature stabilizes (at least one hour). In this way, the temperature of the water and the crucible is brought to that of the machine, so that the shelf temperature does not undergo an abrupt disruption when the crucible is placed in the machine to begin ice growth.

After at least one hour of pre-chilling, growth is seeded by shock-freezing the end of the crucible using a solution of dry ice in methanol. A solution of dry ice in methanol is used to shock-freeze the bubble

at the end of the crucible. (Dry ice sublimes at –78 °C; since the freezing point of methanol is below –78 °C, a mixture of dry ice and methanol will stay at –78 °C, which is past the temperature that water can supercool to.) The crucible is then placed in the machine and growth is continued using a computer program to lower the crucible throughout the machine.

3.1.4 Growth Termination

While the ice is growing, the focus is on monitoring all of the growth conditions to make sure that nothing fails. Primarily, this involves checking the shelf temperature to make sure that the temperature is consistently at –0.5 °C and that there are no large temperature spikes (greater than ±2 mK).

To grow a full length boule takes slightly under a full week. After growth ends, the crucible is pulled out of the machine and taken to the sink. The outside of the boule is melted by holding the crucible on its side and gently shaking it to encourage the melted water to pour down the walls. This should not take more than a few minutes; the boule is then placed in a pre-chilled container and placed in the freezer. It should be left to cool for one day before handling.

3.1.5 Computer Controls

Table 1. List of commands used in HyperTerminal and their corresponding actions.

Command	Explanation
1!	The bang (!) command gives the number of microturns per step. In this case, there is one microturn per step.
253?	This asks the computer how many microturns per step the motor will be or is going. The response, assuming the 1! command prior, will be 253,1.
0e	Since the bang command disrupts communication between the computer and the controller, the 0e command is used to restart the communication.
10r	The r command indicates the number of steps per second. In this case, the motor makes ten steps per second—that is, one step every 100 milliseconds.
-10?	This asks the computer how many steps the motor will be or is taking per second. The response, assuming the 10r command prior, will be -10,10.
5800000g	The g command (g for “go”) instructs the motor to make that many steps. In this case, the motor will take 5.8 million steps and then stop rotating.
-1?	This asks the computer what position the block is at. A response of -1,46 would mean that the block has moved 46 steps.
-s	The -s command (s for “slew”) tells the motor to bring up the block.
z	The z command stops the motor, whether it had been operating under the g or the -s control. In the latter case, wherever the machine stops becomes the 0 position. As such, this control is used prior to beginning growth in order to recalibrate the starting position.

A LabVIEW program monitors and controls the temperature of the modified Bridgman-Stockbarger apparatus using a proportional-integral-derivative (PID) controller. The program provides the option of logging both the room temperature and the shelf temperature, so that the cause of a defective crystal can potentially be attributed to temperature control flaws if any occur. The setup gives ±2 mK temperature control provided that the room temperature does not fluctuate drastically.

An additional LabVIEW program is utilized for communication between the computer and the stepper-motor of the Bridgman apparatus. The program allows modification of the step rate, the number of microturns (i.e. the number of fractional rotations the motor makes in order to complete a full rotation), and the number of steps. Table 1 lists the commands used throughout the ice growth process; they are listed in the order that they would be given to the computer.

3.1.6 Adjusting the Shelf Temperature

One of the unfortunate issues with the ice-growth machine is that the temperature set point and the actual temperature differ. That is, a shelf set point of 0 °C does not necessarily mean that the shelf temperature will be at 0 °C, nor would that even ensure that growth occurs specifically at the shelf.

In identifying what the appropriate shelf set point needs to be to keep the growth front at the shelf, two attributes are critical: (1) the position of the growth front, and (2) the shape of the growth interface. The rationale for keeping the growth front at the shelf is that the temperature is the most controlled there; the only two temperatures that are controlled within the machine are that of the shelf and the outer bath, so the shelf is the best point of access for controlling ice growth.

A crucial step in confirming the location of the growth front is to observe and measure the position of the ice-water interface at the end of growth. This is done by stopping the motion of the crucible and removing the crucible from the machine. The position of the ice-water interface is measured and compared against the expected value for the amount of ice grown at the conditions being used. If more ice has grown than expected (e.g. the ice level is 9.0 cm up, whereas the calculation had predicted 8.6 cm of growth), then the shelf set point is too low (the machine is too cold) and needs to be raised.

The other aspect to consider in the analysis is the shape of the ice interface. Ideally, the growth interface is flat. However, if the shelf and outer bath are not calibrated appropriately, other shapes may be possible. For example, it is possible to obtain triangular growth fronts, where the center of the boule was evidently colder than it should have been and resulted in more growth in the center of the boule than at the edges. In these situations, it is not just the shelf temperature that needs to be considered, but the chiller temperature as well.

3.1.7 Probe Analysis

The other method of analyzing the bath conditions is to use a resistance temperature detector (RTD) probe to measure the temperature throughout the machine. The analysis is best used as a comparison tool against proper growing conditions to determine which parameters need to be adjusted in order to modify ice growth.

The probe analysis is conducted as follows: an RTD probe is inserted through glass tubing such that the probe head is the only part of the probe outside the bottom of the tubing. At the top, the wiring is taped to the glass so that the probe head remains in place at the bottom. A rubber stopper is placed on the tubing to enable the apparatus to be held by the motor box. The position of the stopper is then adjusted along the tubing so that the probe head is just barely touching the top of the ethylene glycol bath when mounted.

The RTD probe is attached to a voltammeter and computer to monitor the temperature as the probe descends with one measurement every ten seconds. It is important that the exact time on the RTD computer is recorded when growth begins; the time difference between the ice growth machine computer and the RTD computer needs to be taken into account when using the .log files to convert elapsed time to distance. The distance from the top of the ethylene glycol to the top of the shelf is also needed; this can be measured most easily and most accurately by placing a ruler in the bath to measure the distance from the top of the machine to the top of the ethylene glycol, and the distance from the top of the machine to the top of the shelf.

The probe should be descended at 1! 1592r to 6000000g, which takes approximately one hour. The resulting data can be presented in a graph showing bath temperature as a function of depth, with the shelf position indicated (the shelf itself is 0.75 inches long). Once again, this graph is best used as a comparison against previously made graphs. An example is presented in Section 4.4.2.

3.2 CRYSTAL CHARACTERIZATION

Though being able to grow single-crystal ice is, in and of itself, an accomplishment, the ice is actually the center of analysis. There are a variety of methods that are used in our laboratory for characterizing the ice after it has been grown in order to better determine the trends in ice growth.

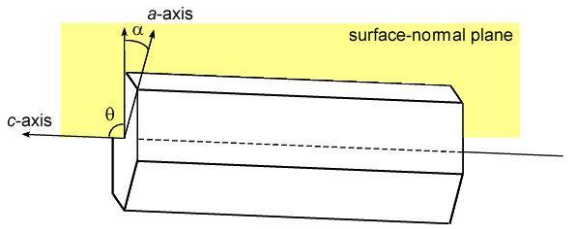

Figure 8. The *c*-axis tilt θ and *a*-axis roll α.

In particular, the methods outlined below are employed as a way to determine the two angles shown in Figure 8. The first angle is the *c*-axis tilt θ, which is the angle between the growth axis and the *c*-axis. Essentially, it describes how far the hexagonal structure of the boule is tilted from the boule and growth axis. The second angle is the *a*-axis roll α, which is the angle between the line formed by the intersection between the basal face and the surface-normal plane, and the *a*-axis.

By definition, $0° \leq \theta \leq 90°$ and $-30° \leq \alpha \leq 30°$. Under these definitions, a basal face is characterized by $\theta \leq 45°$. For both prism faces, $\theta > 45°$; a primary prism face occurs for $20° \leq |\alpha| \leq 30°$ and a secondary prism face for $0° \leq |\alpha| \leq 10°$. By analyzing an etch pit to determine θ and α, it can be concluded which face is exposed and even the angles of rotation needed to reach a specific face.

3.2.1 Rigsby Stage

In 1951, George Rigsby published an analysis of ice samples from the glaciers at Mount Rainier.[36] His analyses were done by placing ice samples in between a set of crossed polarizers such that the light passing through was refracted based on the orientation of the *c*-axis in the ice sample. In particular, he used a rotation stage to precisely measure the location of the *c*-axis. The Rigsby stage, as it is now called, is capable of easily differentiating between domains in an ice sample. If secondary domains are present, they are easily spotted and noted, as shown in Figure 9.

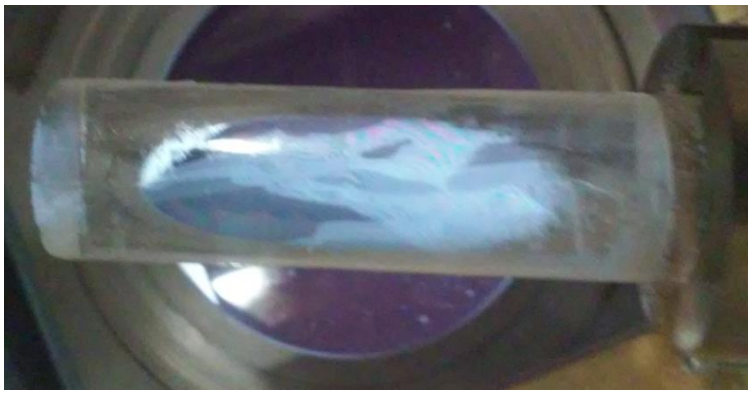

Figure 9. A demonstration of how multiple domains can easily be spotted within the crossed polarizers. Each shaded area corresponds to a separate domain; this boule does not have a particular dominant domain.

In particular, the Rigsby stage can be used to determine the orientation of the *c*-axis within the sample. This feat utilizes the fact that when the *c*-axis is oriented vertically, a thick, black stripe can be seen. Rotating the boule 90° from the position of this dark extinction band (in either direction) and then within the plane of the polarizers causes the boule to go entirely extinct; the *c*-axis is now oriented horizontally. Rotating 180° from a particular orientation gives the same refraction pattern in the stage, though the direction of the vector is flipped.

(a) **(b)**

Figure 10. Extinction events that occur with the *c*-axis oriented (a) vertically and (b) horizontally.

3.2.2 Saw Fixture

To cut the ice, the boule is mounted in a custom-made mount that slides along a guide rail. The mount has two degrees of rotation; the laboratory axes X, Y, and Z are defined accordingly (Figure 11). There is a rotation about the boule axis, when the boule is mounted, and that is defined as a rotation about Z, such that

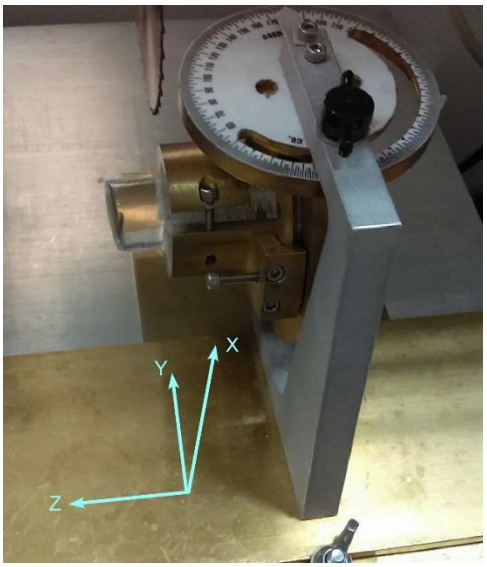

Figure 11. Laboratory axes X, Y, and Z, as related to the saw fixture and sample mount.

the boule axis coincides with the laboratory axis Z. The mount itself can also swing back and forth, and that is described as a rotation about X, such that the X axis is the one that runs out of the freezer towards the user. The Y axis remains, defined such that the positive Z axis runs to the left in the freezer, according to the right-hand rule.

By convention, the boule always begins mounted with X at 180°. This position orients the boule along the Z axis. When X is at 90°, the mount in which the boule is in can be slid to rest within the Rigsby stage. Figure 12a shows the X rotation mount from an overhead view. The black knob locks the mount in place. In Figure 12b, the Z rotation mount is pictured from the right (the X mount rests above it). The Z mount is secured by two screws on the opposite side. Typically, a small mirror is used to read the Z position.

The saw itself lies along the Y axis, such that it cuts along the XZ plane. The saw should be turned on for two minutes prior to the first cut to allow the motor to warm up. After the first cut, a ruler is placed down along the edge of the rail; in this way, the plate can be moved 1 cm. Since the thickness of the blade's cut is about 2 mm, this will produce an 8 mm thick sample. This thickness works very well, for it allows multiple analyses to be performed on the same sample before the ice anneals away. Additionally, it is simply a convenient thickness to work with—something smaller would slip more easily.

(a) **(b)**

Figure 12. The rotation mount along (a) X and (b) Z.

3.2.3 Microtoming

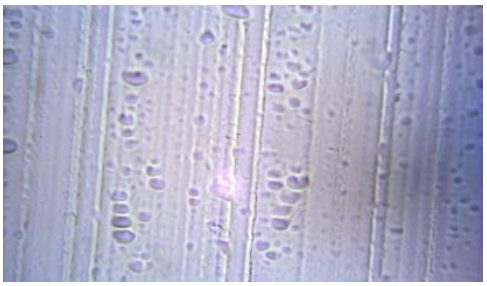

Figure 13. Example of the excessive striations present on an ice surface after microtoming with an old razor blade.

Etching requires a flat surface. To cut a flat surface on an ice sample, an American Optical Rotary model 820 microtome is used. The microtome uses CL Sturkey diamond-coated disposable razor blades to cut micrometer-thin slices off a mounted ice sample. The razor blades must be replaced periodically, otherwise abundant striations will be left by the razor blades. These will be visible when the ice is placed under the microscope, and they leave the surface too rough to be flattened out just by self-anneal.

3.2.4 Formvar Etching

The procedure for etching ice was refined in 1958 by Higuchi[37] for the analysis of ice crystals and has since been placed into practice by a number of groups for the purpose of analyzing ice.[38–40] The etching is done by coating the ice sample with 2% polyvinyl formal (Formvar) dissolved in ethylene dichloride. The polymer induces sublimation; as the ice sublimes, it does so in a pattern that leaves behind etch pits.

The best way to visualize the shape of an etch pit is by virtually embedding a hexagonal prism into the ice surface, as shown in Figure 14. When the prism is removed, it leaves behind an imprint that gives rise to the shape of the etch pit. This simulation explains the profile is of an etch pit is represented by profile A and why profile B is never seen, for profile B corresponds to a prism that has been embedded too deeply and created an overhang (etch B), which is high in energy and therefore unstable.

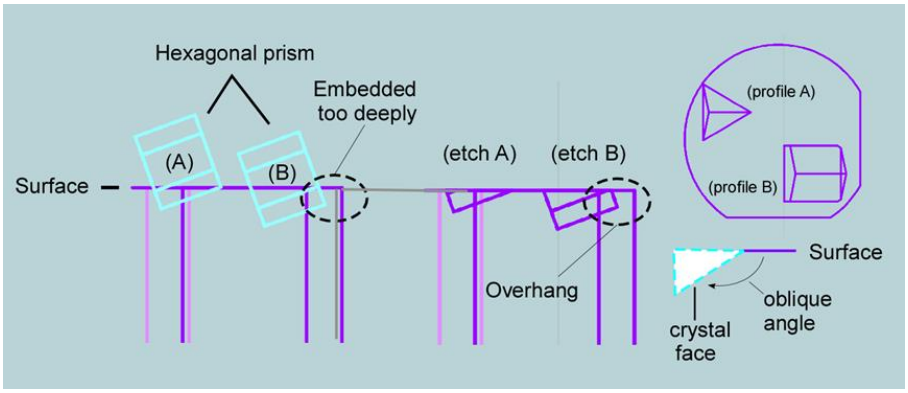

Figure 14. Visualization of how the hexagonal structure of ice gives way to etch pit shape. Etch pits can be simulated by embedding a hexagonal prism in the surface and then removing it to leave behind a negative imprint.

The pits are imaged using a Meiji ML9300 microscope at 10x magnification and a PixelLink PL-A662 camera. 10x magnification captures a view of the size 0.70 mm × 0.56 mm; based on these measurements, the etch pits that are produced range from 25 µm to 100 µm in length. Though the freezer in which the microscope is placed is at –18 °C, the microscope stage is heated to –5 °C to accelerate etch pit formation.

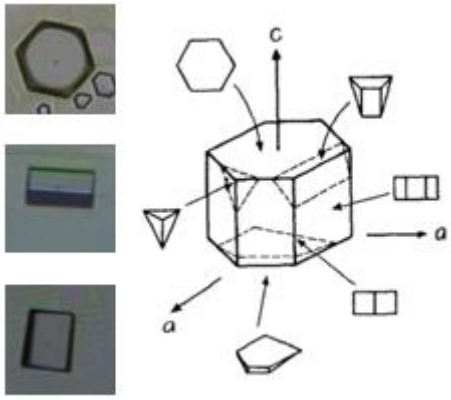

Figure 15. Examples of nearly perfect basal, primary prism, and secondary prism face etches. The diagram on the right is reproduced from Ref. 37 and shows how different etch pit geometries correspond to the hexagonal prism.

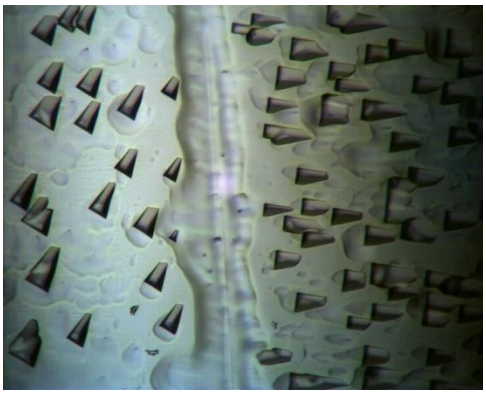

Figure 16. Etched sample containing two single-crystal domains. The grain boundary between them is composed of amorphous ice. (Image reproduced in Ref. 13.)

The analytical utility of this technique is that the geometry of the etch pits that are produced can be used to determine the *c*-axis tilt and *a*-axis roll and therefore indicate the face that is exposed. Figure 15 provides examples of nearly perfect basal, primary prism, and secondary prism face etches, while Figure 16 shows etch pits that are commonly seen for cross sections—that is, etch pits that do not correspond to an exact face, but rather frequently exposed faces with high Bravais-Miller indices. Figure 16 also shows what the grain boundary between two single-crystal domains looks like.

3.2.5 Full Procedure

Prior to the start of the analysis, the boule is glued to a polycrystalline ice handle by placing both pieces of ice in a tube and injecting water between the two pieces to freeze. The purpose of the handle is to be able to place the sample within the saw fixture and thus expose the entire single-crystal sample for cutting and analysis. The polycrystalline handle is grown in a cylindrical Teflon tube whose diameter matches that of the crucible diameters. Attaching the single-crystal boule to the polycrystalline handle is done by cutting a flat edge on both pieces of ice, and then placing them in a cylindrical tube of slightly larger diameter. The tubing has a number of small holes through which water can be injected; by placing the two pieces of ice against each other, they can be fused together as the injected water freezes to both flat ends.

Once the two pieces have been frozen together, the entire sample is removed by melting the outer layer. This is done simply by holding the tubing within the freezer until the warmth from the person's hands melt the outside of the ice. The rest of the ice remains frozen, and by employing a Teflon stick to push the ice out of the tubing, a minimal quantity of ice is lost in the process. Any remaining holes are patched up with water, and the boule is left to freeze for at least a day before handling.

When the boule is ready to be used, it is mounted in the saw fixture and the appropriate slice is cut. The bottom of the cross section is then flattened against sand paper on a flat, glass surface. A microscope slide is then selected such that if there is a reference flat (an edge that marks the orientation of the sample with respect to the original boule), it is placed along a guide on the appropriate side, and the sample is

placed on the slide. Gluing the sample to the slide entails keeping two fingers underneath the slide to slowly warm up the sample until a film of water can be seen beneath it; at this point, the slide is carefully and evenly placed down and the water is allowed to solidify, thereby "gluing" the sample to the slide. The sample is left for twenty minutes so that the newly form ice fully solidifies.

After twenty minutes, the slide is placed on the microtome fixture and onto the microtome. Ten slices at 25, 15, 5, and 2 μm each are cut. The slide is then placed on the microscope stage and allowed to self-anneal for at least twenty minutes; the progress can be monitored with the camera. A striation left by the razor blade of the microtome should be located prior to allowing the sample to self-anneal, so that the error in gluing the sample onto the slide perfectly can be determined. The angle between a perfectly vertical line and the razor blade striation gives the rotation of the sample on the slide. Each photo is then rotated by this angle to ensure that a vertical line on the image is truly vertical.

A typical, full-length boule is approximately 9 cm in length. Each sample requires a thickness of 1 cm, so approximately 9 cross-sections can be cut out of one boule. However, if a particular face is chosen, the rotation of the boule will be such that additional length will be needed. As such, a basal face typically requires 3 cm of boule, and primary and secondary prism faces require 1 to 2 cm. Therefore, the minimum boule length that is needed to analyze a cross-section, basal, primary prism, and secondary prism faces is 7 cm.

4 RESULTS

4.1 FACE STABILITY AT THE ICE-WATER INTERFACE

The results presented in this section were previously published in *The Journal of Physical Chemistry B*.[13]

4.1.1 Face Stability

Because the interfacial energies of each of the faces of ice are very similar, the face that is favored is especially sensitive to the conditions under which the ice is grown. In particular, the growth methodology plays a role in determining which face dominates at the growth interface.

To interpret which face is the most stable when ice is grown from the melt at thermodynamic equilibrium, 23 samples were analyzed by etching boule cross sections. I analyzed 11 of the 23 samples; their orientations are presented in Table 2. The etch pits immediately characterized the exposed face and further analysis revealed the *c*-axis tilt and *a*-axis roll. For the 23 samples, it was found that the secondary prism face surfaced 61% of the time, followed by the primary prism and basal faces (39% and 17%, respectively). Nearly single-crystal boules were included in the count for the basal face, but not for the primary or secondary prism faces. There were 18 single-crystal boules and 5 boules that had two single-crystal domains.

Table 2. Summary of the 11 ice samples that were analyzed. Etch images were captured at 10x magnification; the square images are 82 μm × 82 μm. When two numbers are listed, they each represent one single-crystal domain in a boule with two single-crystal domains.

Boule	Domains	*c*-axis tilt, θ	*a*-axis roll, α	Growth Face	Etch Image
102	1	15°	8°	basal	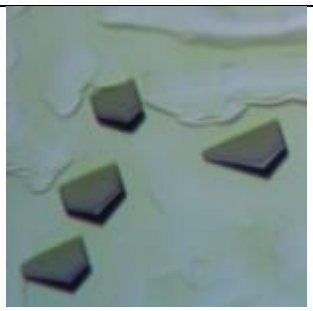
103	1	65°	0°	secondary	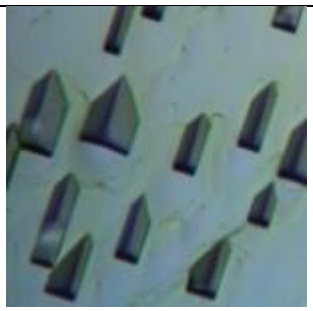

104	2	40°	5°	basal	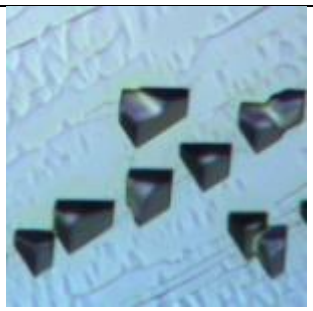
105	1	>89°	6°	secondary	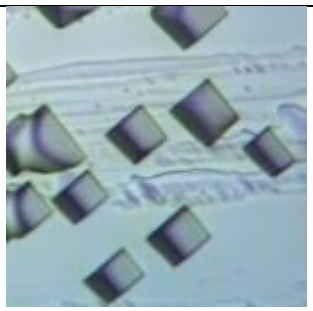
106	2	83° 85°	<1° 30°	secondary primary	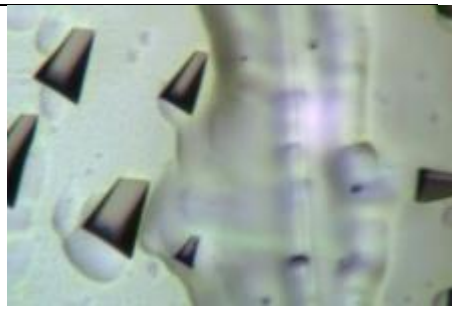
107	1	85°	<1°	secondary	
108	1	55°	<1°	secondary	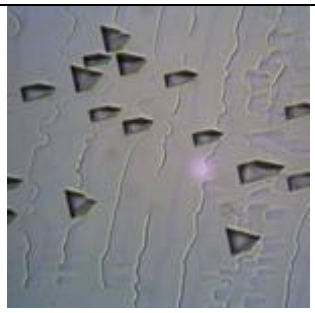

109	2*	85°	30°	primary	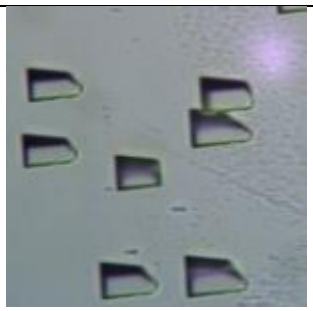
110	1	85°	30°	primary	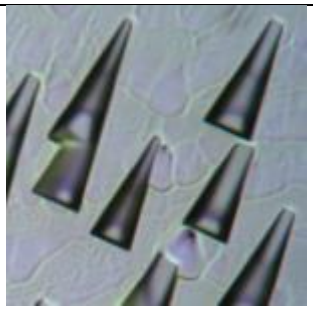
111	2*	85°	30°	primary	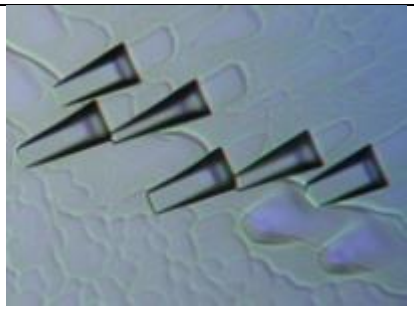
112	1	85°	30°	primary	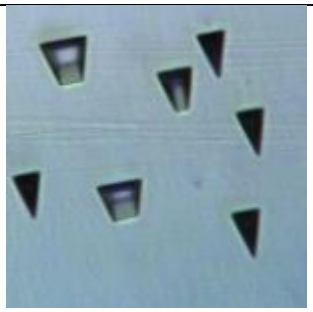

*The second domain was present along the wall of the crucible.

4.1.2 Boule Orientation

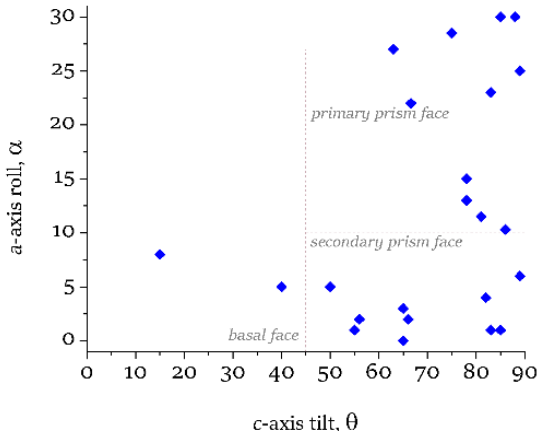

Figure 17. Plot of the *a*-axis roll and *c*-axis tilt for all the boules used in this paper and through August 2015.

Since the publication of the paper, more boules have been grown. Figure 17 shows the boule orientation for all the boules included in the paper, along with more recent ones up through August 2015 (at which point the machine was modified for the growth of D_2O ice). The data comes from mixed growth conditions; while the boules presented in the paper were grown at 2! 2r, the procedure was first modified to grow at 1! 4r and then at 1! 10r.

Nevertheless, it is apparent that there is a preference for the prism faces. With the exception of two boules, all were prism or pyramidal faces—and the two that were basal faces were grown at the "inferior" 2! 2r conditions used in the first paper. The change to 1! 4r showed both an increase in single-crystal yield and a disappearance of the basal face at the surface. In addition, the preference for the secondary prism face exhibited in our original data has since dwindled, and the primary prism face occurs more frequently. Although whether the primary or secondary prism face is more stable is slightly unclear from the data, the trend of the secondary prism face still dominates with the addition of new data points. Thus, the conclusion of the paper remains valid under the improved growth conditions.

4.2 Producing Desired Ice Faces

The results presented in this section were previously published in the *Proceedings of the National Academy of Sciences*.[16]

For a long time, the question of how our laboratory arrangement could be used to isolate any desired face posed a challenge. The difficulty in only having two rotations available limited the feasibility of the task. In the end, the rotations necessary to isolate any face from the original exposed face were identified.

4.2.1 Identifying the *c*-Axis

On the day of the analysis, the boule is mounted in the saw fixture (the handle is placed within the jaws of the fixture, so that the single-crystal boule is fully exposed). The fixture is then rotated so that the boule can be viewed within the Rigsby stage and the *c*-axis is located as follows. First, the Z angle of the extinction band is recorded, and the boule is rotated approximately 180° to locate the band on the opposite side of the sample, so as to confirm the first reading and produce a more precise measurement. The boule is then rotated 90° in Z from either extinction band. The boule is then rotated in X until fully extinct; if this requires a negative ΔX, then the boule is rotated 180° in Z and the extinction position relocated so that ΔX is positive. The *c*-axis tilt is given by 90° − ΔX.

The Z angle at which the positive ΔX is recorded is used as home Z; a reference flat is cut (only slightly longer than 1 cm in length) with the saw fixture at home Z and X = 90°, such that the left side of the sample is flat. Before the sample is cut, the boule is marked with an arrow pointing towards the end of the boule, so that when the sample is glued onto the slide, it is known that the side closer to the end of the boule is the one that gets placed face down on the microscope slide.

4.2.2 Determination of θ and α

The first step in the process of cutting a selected face is determining the *a*-axis roll, α, and the *c*-axis tilt, θ. The tilt can be located by using the crossed polarizers in the Rigsby stage. Both angles can be found by etching a cross-section and then using a mathematical formulation to calculate α and θ. The roll can also be identified by etching a basal face. The most accurate results come from using all three methods in tandem. Although the determination of θ in the crossed polarizers is effective, it is unable to determine α. Thus it is still necessary to etch a cross section, which provides the advantage of both determining α and confirming the value of θ.

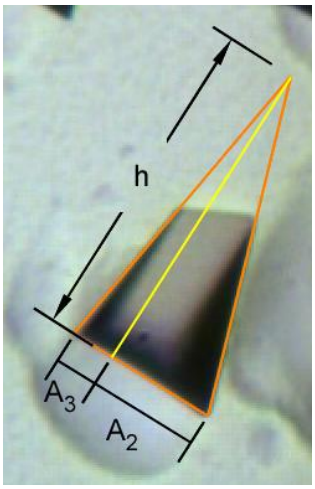

Figure 18. Definitions of A_2, A_3, and h, the three parameters used to find α and θ.

The two angles are determined by drawing a triangle around the trapezium etch pits seen in the cross section etch. The triangle determines three values that are then used to calculate α and θ. As shown in Figure 18**,** the three values are h, the height of the triangle drawn by extending the sides of the trapezoid, and A_2 and A_3, which are formed by the bisection of the base of the triangle by the height. Define the ratio $R \equiv A_2/A_3$ and let $b = \tan 60°$. The two angle formulas are given by:

$$\alpha = \tan^{-1}\left[\frac{(b^2+1)(R+1) \pm \sqrt{(b^2+1)^2(R+1)^2 - 4b^2(R-1)^2}}{2b(R-1)}\right]$$

$$\theta = \cos^{-1}\left[\frac{(A_2+A_3)/h}{\tan(60°+\alpha)+\tan(60°-\alpha)}\right]$$

The best way to determine α uses a basal face etch. The basal face is cut using the formulas given in Section 4.2.3, and then the *a*-axis roll is found by looking at the rotation of the basal face hexagonal etch pits with respect to a perfectly upright hexagon. The process is demonstrated in Figure 19. A basal face etch pit is located and then a hexagon is placed over it in a drawing program (Canvas 12). The set of axes that correspond to the hexagon are added, along with a horizontal line. The angle between the horizontal line and the closest hexagonal axis determines the *a*-axis roll. If the axis is located counterclockwise from the horizontal line, that gives $\alpha < 0$; conversely, if it is located clockwise, $\alpha > 0$. This method is more accurate than the cross-section etch pit method for determining α, since the roll angle is difficult to visualize in the wide variety of cross-section etch pits.

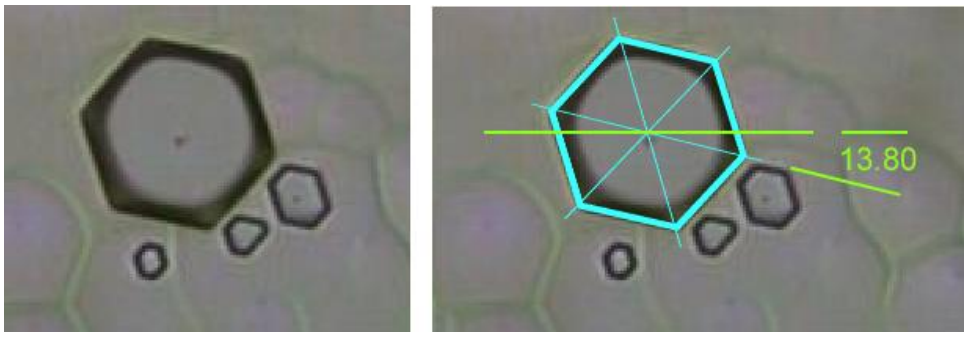

Figure 19. Example of how the *a*-axis roll is determined for a basal face etch pit. The original etch pit is shown on the left; on the right, a hexagon is overlaid with axes. A horizontal line is drawn in green, and the angle between the horizontal and the nearest hexagonal axis is found to be +13.80°.

4.2.3 Selected Face Rotation Angles

Once the two angles α and θ have been identified, rotations in the laboratory X and Z axes are required in order to expose the desired face. The starting ("home") values for the angles in X and Z are X = 90° and Z at the angle that gave the full-boule extinction in the Rigsby stage. These rotations describe the angle by which X and Z need to be adjusted from the home values. For the basal face, no Z rotation is required, and the X rotation is $90° - \theta$. For the prism faces, define:

$$\gamma \equiv \begin{cases} +30° & \text{primary prism face,} \quad \alpha < 0 \\ -30° & \text{primary prism face,} \quad \alpha > 0 \\ 0 & \text{secondary prism face} \end{cases}$$

Then rotate about Z by η and about X by ξ:

$$\eta = 180° + \tan^{-1}\left[-\frac{\tan(\alpha+\gamma)}{\cos\theta}\right]$$

$$\xi = \tan^{-1}[\cos\eta \tan\theta]$$

4.3 Atypical Etch Pits

The Formvar etching technique was initially used primarily to study natural ice, and much of the literature on the topic features basal face etch pits. It is unusual to see many examples of prism or pyramidal faces in early papers of the topic. The ability to etch any face of ice now has led to new insights that surpass previous exploration of ice etching and raise questions about the interfacial energies of the various faces of ice.

4.3.1 High Index Faces

After the publication of the paper presented in Section 4.2, it became possible to prepare a (nearly) perfect primary prism face sample. While there had always been the ability to roughly cut some sort of prism face, precisely locating it had been difficult (and therefore prone to error) using just the Rigsby stage.

Interestingly enough, when these perfect primary prism faces were etched, the anticipated rectangular etch pit exhibited modifications in the form of chamfered corners, as shown in Figure 20. The octagonal shape of the etch pits shown in Figure 21 occurred in approximately one-third of all etch pits on each primary prism face. These corners are high-index faces that modify the corner normally formed by the basal and primary prism faces; their appearance implies that the high-index faces are not significantly higher in energy, and also that the corners of an etch pit become too high in energy to sustain at larger etch pit sizes.

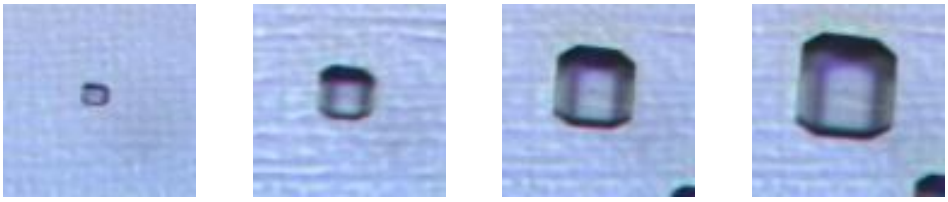

Figure 20. Development of a primary prism face etch pit.

Furthermore, even the etch pits that remained rectangular were modified. As Figure 22 shows, there are dark (nearly black), gray, and light areas. This shading actually enhances our ability to analyze the etch pit structure and clearly shows the faces involved in a primary prism face etch pit. The two dark sides are basal face walls, where the trapezoidal shape indicates that the bottom half of the hexagonal design of a basal face is exposed. The 120° angles of a hexagon are easily spotted. The gray and light boxes are also trapezoidal because they are rectangular but viewed from above at an angle; thus they are the expected primary prism face walls of the etch pit.

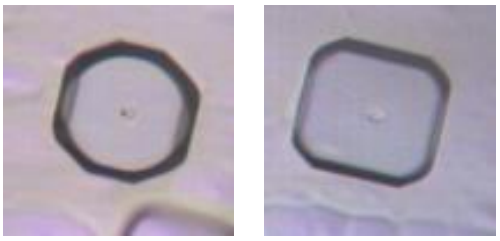

Figure 21. Octagonal etch pits, which can be viewed as the expected rectangular etch pits with chamfered corners.

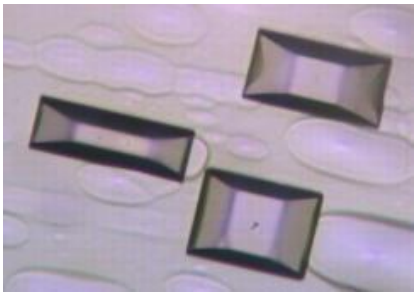

Figure 22. The extensive internal shading that is present in some primary prism face etch pits.

There is precedence for high-index faces; a group at the University of Puget Sound imaged ice single crystals grown inside an environmental scanning electron microscope (SEM).[41] In 2010, they published a paper reporting the $\{10\bar{1}1\}$ and $\{20\bar{2}1\}$ faces in growing and ablating crystals, the former of which was confirmed via molecular dynamics simulations. Figure 23 shows their SEM images, with the basal and primary prism faces clearly labelled. The chamfered corners connecting the two are also indicated.

As a final note, one of the reasons for looking at the primary prism face had been to apply the Wulff construction to our ice. The primary prism face is convenient for this task, since primary prism face etch pits are formed by exposed surfaces of primary prism and basal faces, the area of which can be calculated for each. Although all etch pits are formed by these faces, not all of them present the faces in such a way

as to be able to calculate area. For example, a basal face etch pit features six primary prism faces, but all viewed at a 90° angle, such that there is no indication of the depth of the etch pit. However, it has become increasingly clear that there are more faces involved in the formation of these etch pits than just the primary prism and basal faces. The Wulff construction thus becomes too complicated, with at least three or four different types of faces involved.

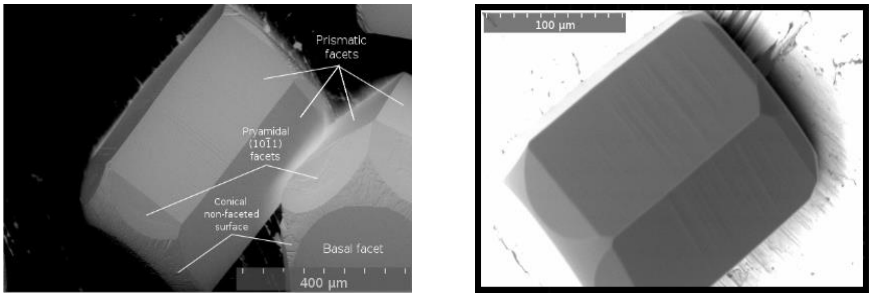

Figure 23. SEM-grown single-crystal hexagonal ice, imaged by an SEM, showing pyramidal $\{10\bar{1}1\}$ faces between the basal and primary prism faces. (Images taken from Ref. 41.)

4.3.2 Basal Face Irregularities

When a nearly perfect basal face is etched, some etch pits grow asymmetrically. The etches displayed only hexagonal shapes, but the final shapes were not regular hexagons and instead featured, as shown in Figure 24a from left to right: elongated hexagons, where two edges were more elongated than the other four; triangles with cut corners; and other hexagons with no regular pattern. The types of shapes present in one area were not all uniform, such that a full variety of etch pits could be seen in one image (Figure 24b).

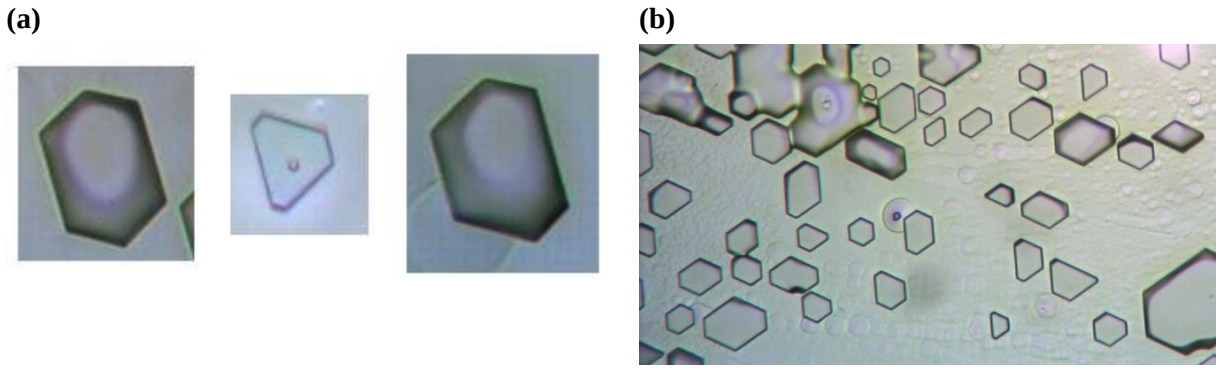

Figure 24. Examples of basal face etch pits

It is possible that these irregular basal face etch pits are simply sensitivities to the surface morphologies on which they grow; rough surfaces cause irregular etch pit growth. To attempt to eliminate the possibility of the basal face shape having been due to a rough surface, the samples were left to anneal for longer periods of time on the microscope stage (30 to 40 minutes instead of the usual 20 to 30 minutes). The same irregular shapes were still seen.

4.4 D_2O Ice Growth

4.4.1 Procedural Modifications

Section 2.2 addresses the theoretical concerns of growing D_2O ice. The following procedures account for the thermodynamic differences with deuterated water, as well as the issue of growing ice efficiently and effectively.

The primary change to the procedure appears at the degassing stage. The crucible is placed on the vacuum line; in lieu of using Teflon tape to cover the crucible and protect the water within it from dust, a septum cap is placed on the crucible to seal it off from the atmosphere. The septum cap is pierced with a needle that is attached via Tygon tubing to the vacuum line. Prior to beginning the degassing, the air above the deuterated water is pumped off (once again, the minimal pressure is kept at 20 torr, but the inlet is attached to nitrogen rather than being open to the atmosphere) and replaced with nitrogen. This process is repeated thrice, and then the two-hour degassing step commences. Once degassing is finished, the crucible is once again filled with nitrogen to a final pressure of slightly over an atmosphere to minimize the entrance of H_2O.

The ice-growing machine is also modified. To account for the higher freezing point of D_2O, the shelf temperature is set to 3.55 °C. Reasons why there is an increase of 4.05 °C from what is used for H_2O, rather than 3.82 °C, are discussed in Section 2.2. The bath temperature is set to 1.60 °C on the chiller; the computer reads the temperature in the outer bath to be 1.08 °C.

The correct temperature was found by originally increasing the temperature by 3.82 °C and then making small changes to the shelf and bath temperatures until the amount of ice present in the boule at the end of growth was (i) equivalent to the expected amount, as calculated with the step rate, step size, and number of steps, and (ii) relatively flat at the top (as fully discussed in Section 3.1.6).

The final parameter that is different is the growth rate. Instead of growing at 1! 10r, D_2O ice is grown at 1! 4r. At that rate, a full-length boule takes sixteen days to grow.

4.4.2 Probe Analysis

One way of analyzing the conditions of the ice machine is by considering the temperature gradient throughout the bath. There is a subtle requirement that the gradient be neither too steep nor too shallow, and the gradient has indeed been found to have effects on the yield of single crystals.[5] For example, with H_2O ice, 100% yield came only after modification to the shelf and bath temperatures.

The standard way of analyzing the temperature gradient is outlined in Section 3.1.7. The method is crude; it does not incorporate the effect of having a crucible traverse the bath, nor does it involve ice growth. It is simply meant to gain an understanding of the temperature gradient within the machine overall, irrespective of the influence that growing ice has on the temperature. With D_2O ice, this method provided the starting point for the shelf and bath temperatures. After adjustments were made to finalize the conditions needed to grow D_2O ice, the method was repeated. This allowed the resulting plot to be used to compare

D_2O ice growth conditions against those for H_2O ice; the comparison is shown in Figure 25. The most notable difference is that the temperature gradient at the shelf is much shallower (half as steep) for D_2O than for H_2O. This implies that D_2O ice growth is much more sensitive than that of H_2O; this is further confirmed by the fact that D_2O ice must be grown at a slower rate.

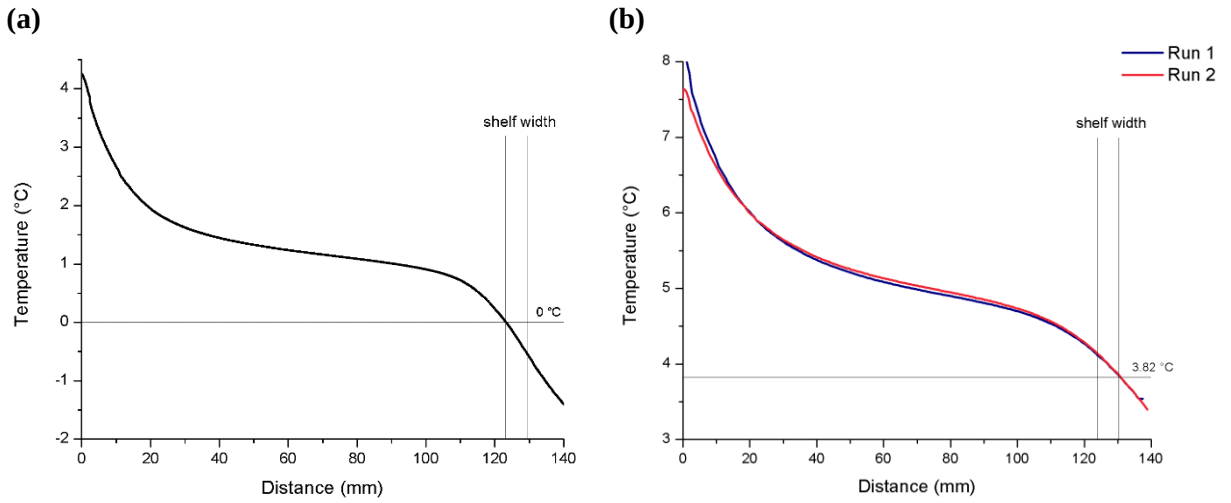

Figure 25. Probe analysis of ice growth machine conditions for (a) H_2O ice growth, shelf T = –0.5 °C, versus modified conditions for (b) D_2O ice growth, shelf T = 3.55 °C. The temperature gradients at the shelf are –0.088 °C/mm and –0.044 °C/mm, respectively.

The difficulty in doing a probe analysis during ice growth is that inserting a probe into the boule would likely negatively impact the environment of the water within the crucible. Instead, we settled upon placing five probes on the exterior of the crucible. They were held in place by one to two layers of Saran wrap; the minimal amount of wrap possible was used, as the wrap affects the thermal conductivity of the system. It was not expected that the resulting boule would be single-crystal, and indeed, it was not; nevertheless, the goal of probing the thermodynamics of the growing boule (in a preliminary fashion) was accomplished.

The five probes were positioned as follows: Probes 1 and 2 were placed along the bulb, approximately 1.3 and 2.5 cm up the length of the crucible, respectively. Probes 3, 4, and 5 were placed along the main section of the crucible, approximately 6.0, 8.3, and 9.9 cm up. All of the positions are approximate, as it was difficult to position the probes horizontally, particularly along the bulb.

Throughout growth, the resistance values measured by the probes were read three times a day at discrete points. Three data points were also taken after the end of growth. The results can be seen in Figure 26, where the resistance values have been converted to temperature. A drastic difference between the temperature progression for the two probes on the bulb versus the three probes along the main section of the crucible can be seen, although all of the probes seem to follow the overall gradient shape presented in Figure 25. The temperature is initially stable, then drops when passing through the shelf region, and finally stabilizes once more after exiting the shelf region.

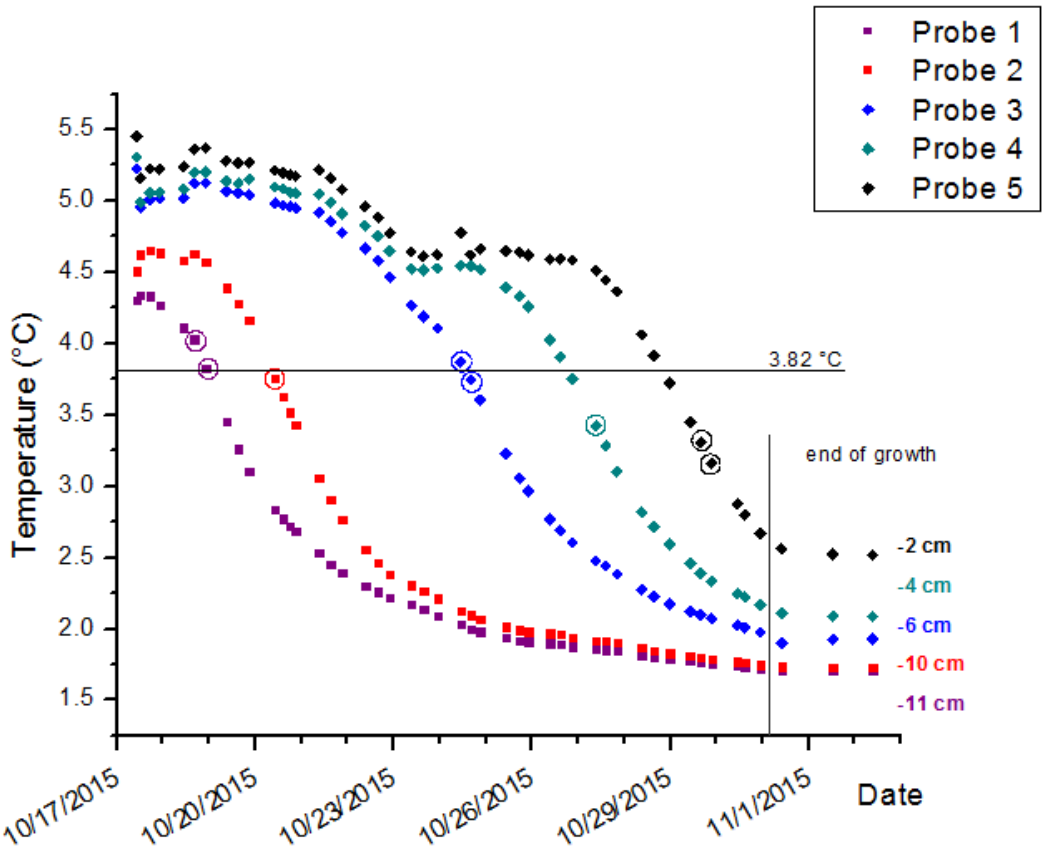

Figure 26. Five-probe analysis of a growing boule of D_2O ice. Probes 1 and 2 (squares) were placed along the bulb; probes 3, 4, and 5 (diamonds) were placed along the main length of the crucible. The circled points correspond to when that area of the crucible was passing through the shelf. The distance values on the right indicate how far below the shelf the probe was at the end of the growth.

One area of note is the stable region at ~ 4.5 °C. It appears that the three probes along the main part of the crucible experience very little temperature change after the start of growth (for about seven days). While probe 3 appeared to enter the shelf region after day 7, the other two probes, instead of also getting colder, stabilized at 4.5 °C until reaching the beginning of the shelf region. This different behavior implies that the heat dissipation in the bulb versus the rest of the boule is different, which is understandable—when the bulb is growing, there is very little ice beneath the growth front. Since ice is more thermally conductive, the water above the growth front has to dissipate more heat than it would otherwise if there were a considerable amount of ice beneath the growth front. By the time growth is occurring in the main portion of the boule, there is a considerable amount of ice beneath the growth front, and most of the heat is likely dissipated through the ice beneath the growth front, rather than the water above it.

This also accounts for the fact that the temperature of the probes when passing through the shelf (the circled points in Figure 26) is colder than 3.82 °C for probes 4 and 5. (Probe 3 was just barely above the neck, so the effect would not be as pronounced for it.) The set point for the shelf temperature, which is set so that the temperature is stable at 3.82 °C, is not able to compensate for the various heat dissipation patterns throughout the growth process. An improved growth technique would be able to account for this

and adjust the shelf temperature as needed so that the growth front is always located exactly at the shelf, exactly at 3.82 °C. What this probe analysis implies is that the further along the ice growth process is, the higher up within the machine the ice is freezing.

4.4.3 D_2O Etching

Just as it is for H_2O, etching is a major point of interest for D_2O. Since etch pits are formed by basal and primary prism faces, the shape of the etch pits can reveal the relative energies of the two faces. The sharp edges of H_2O etch pits indicate that the basal and primary prism faces are significantly lower in energy than the pyramidal faces (although as discussed before, this is not strictly true). For D_2O, the sharp edges and corners are not observed, indicating that the surface energies of the faces are closer in energy than they are for H_2O.

Firstly, it is important to note that D_2O etching requires temperatures due to the higher melting point. The temperature is moderated by measuring the resistance of RTD probes taped to the microscope stage; the resistance is converted to temperature using a LabVIEW program that incorporates the RTD algorithm. A "good" etching temperature is subjective, but the guidelines are that the etch pits grow neither too quickly nor too slowly. Quick growth results in overpopulation of etch pits on the surface, causing the etch pits to grow and merge together before their shape can be studied; slow growth is a nuisance. By etching samples at different resistances and monitoring the etch pit growth rates that resulted, the correct resistance was found to be around 35 kΩ, which corresponds to –1.41 °C. (H_2O etching uses 44 kΩ, which is –5.01 °C.) Note that the resistance is given as a rough value to be used as a target and not as an exact number that needs to be reached for etching to occur. Differences in the rate of etch pit formation are only noticeable for great than 1 to 2 kΩ deviations from the desired temperature.

The D_2O etch pits themselves displayed a few notable differences from those of H_2O (Figure 27). In cross section etches, where the exposed face was arbitrary, the most prominent feature was rounded edges. A very common shape was a hexagon with two or three sharp corners and the remaining corners and edges rounded off.

Figure 27. Examples of cross section etches for D_2O.

One possible explanation for the greater variety and roundedness in etch pit shape is that the inter-facial energies of D_2O ice are much more similar in energy than those of H_2O. It is already known that for H_2O, the energies are similar and are very sensitive to conditions. Similar energies would cause rounding by incorporating more than just the primary prism and basal faces in the etch pit morphology, thus enabling more shapes to be formed. As was seen with H_2O, having one additional face that partakes in etch pit

formation brought the shape from four-sided to eight-sided, as in the case of the chamfered primary prism face etch pits. With more available faces partaking in etch pit formation, the etch pit is able to take on many more sides and shapes. The rounded corners can be construed to be multiple faces.

In fact, if the trapezium formulation of the H_2O etch pits is applied here, it becomes clear that there are additional faces involved. The trapezium construction relies upon the fact that there are only basal and primary prism faces forming the edges of the pits; the only possible shape that can be formed with these two faces is the trapezium, with a hexagon and a rectangle at the two extremes of this. Any intermediate shape can be analyzed with the trapezium construction; note that although in Table 2, the near-basal face etch pits are pentagonal, the construction can easily be adapted by ignoring the two parallel sides rising up from the base. It is truly only with the D_2O etches that the trapezium construction fails, implying that there are different faces at play in the formation of D_2O etch pits.

Unfortunately, the microscope can provide very limited information about the etch pit morphology. An interesting question is what the surface of the bottom of the etch pits look like; if the edges are any indication, then the bottom of the pits are likely rounded and rather spherical, as opposed to being defined by sharp edges. One way to confirm this would be to use differential interference contrast microscopy, the theory of which is discussed in Section 2.3 and the implementation of which is discussed in Section 4.5. Hopefully, the DIM will be able to provide us with the results we so desire about what etch pits look like; the fact that just the top surface, imaged by conventional optical microscopy, can provide so much indicates that a more powerful microscope, not limited by one dimension, will likely provide even more information.

4.5 CONTRAST MICROSCOPY

Differential interference contrast microscopy (introduced in Section 2.3) employs optical interferometry to measure distances on a sample and improve contrast in an image. A differential interference contrast microscope (DIM) was built because the ability to measure distances presents a great advantage to ice surface analysis. The microscopy essentially allows one to construct an image of the surface topology of a sample; one instance in which this would be useful is in measuring the heights of step edges.

Another instance is in analyzing the shape of etch pits; although a standard optical microscope beautifully captures the geometry of etch pits at the etch surface, it reveals little about their three-dimensional structure below the surface. Particularly in the case of the D_2O etch pits described in Section 4.4.3, having knowledge about the structure of etch pits would provide more information about the interfacial energies of various faces. One would expect that having pyramidal faces close in energy to the three main faces would produce rounded etch pits, where the bottom surfaces would be carved out in a rather spherical shape. On the other hand, if the basal and prism faces are significantly more stable, sharp, defined edges would be expected in three dimensions.

The microscope is currently in its early stages of construction. All of the parts have been mounted on an optical table and placed in their correct locations. The next step will be aligning the optics and preparing it for sample analysis. A sample stage will need to be built, initially one that will be able to hold

something like mica or 5° miscut silica. These will be good reference samples and easier to work with than ice while the microscope is still being perfected. When the microscope is ready for ice, the sample stage will need to be modified so that the ice can remain below 0 °C during operation.

4.5.1 Step Edges on the Prism Faces

As mentioned in Section 2.1.3, at one point the question was raised whether or not a reverse Wulff construction could be used to calculate the surface energies of the primary prism and basal faces. One of the prerequisites for this would be primary prism face etch pits produced at equilibrium conditions (although it is possible that this could never be attained in the given context, near-equilibrium conditions would still be an improvement and worth investigating). To this end, a primary prism face was cut and left to self-anneal at –18 °C (the temperature of the freezer), with the intention of etching it at –18 °C.

Interestingly enough, the result of an extended self-anneal was not a flat surface at all, but rather the image seen in Figure 28a, consisting of long "cuts" extending all across the surface in one direction. Etching of this surface produced distorted etch pits that grew along the "cuts" (Figure 28c). If the standard interpretation of the etch pit is used, then the distorted etch pits grow elongated along the basal face. This is in contrast to the normal growth of a primary prism etch pit, in which both the primary prism and basal faces expand, but the basal face maintains the smallest area.

The secondary prism face produced similar results to those of the primary prism face. Extended self-anneal resulted in "cuts," although they extended in two directions, perpendicular to one another (Figure 28b). Once again, etching the surface produced etch pits directly along the "cuts" (Figure 28d).

This provided further evidence for the hypothesis that the "cuts" are step edges that reveal a perpendicular face to that which is on the surface. The primary prism face would feature basal face step edges, while the secondary prism face would feature both primary prism and basal face step edges, since both faces are perpendicular to the secondary prism face. This is consistent with what would be expected of a surface that is some small angle off from a true primary or secondary prism face. Since the higher-index surface face is higher in energy, as the anneal continues, the surface tends towards a lower and lower surface energy by exposing only primary prism and basal faces. A surface with terraces and step edges corresponding to the three major faces would be lower in energy than the original sample.

The above results were seen to hold at –18 °C, but not at –5 °C, which is the typical temperature used when etching samples. At –5 °C, extended self-anneal produced small, circular indentations on the surface that moved along the surface when time lapse images were taken at intervals of 2 minutes apart. It is believed that the presence of the quasi-liquid layer (QLL) at –5 °C is what enables the defects to move around. The QLL at -18 °C is significantly less pronounced than that at -5 °C,[42] which would explain the difference in the behavior of the primary prism face at those two temperatures.

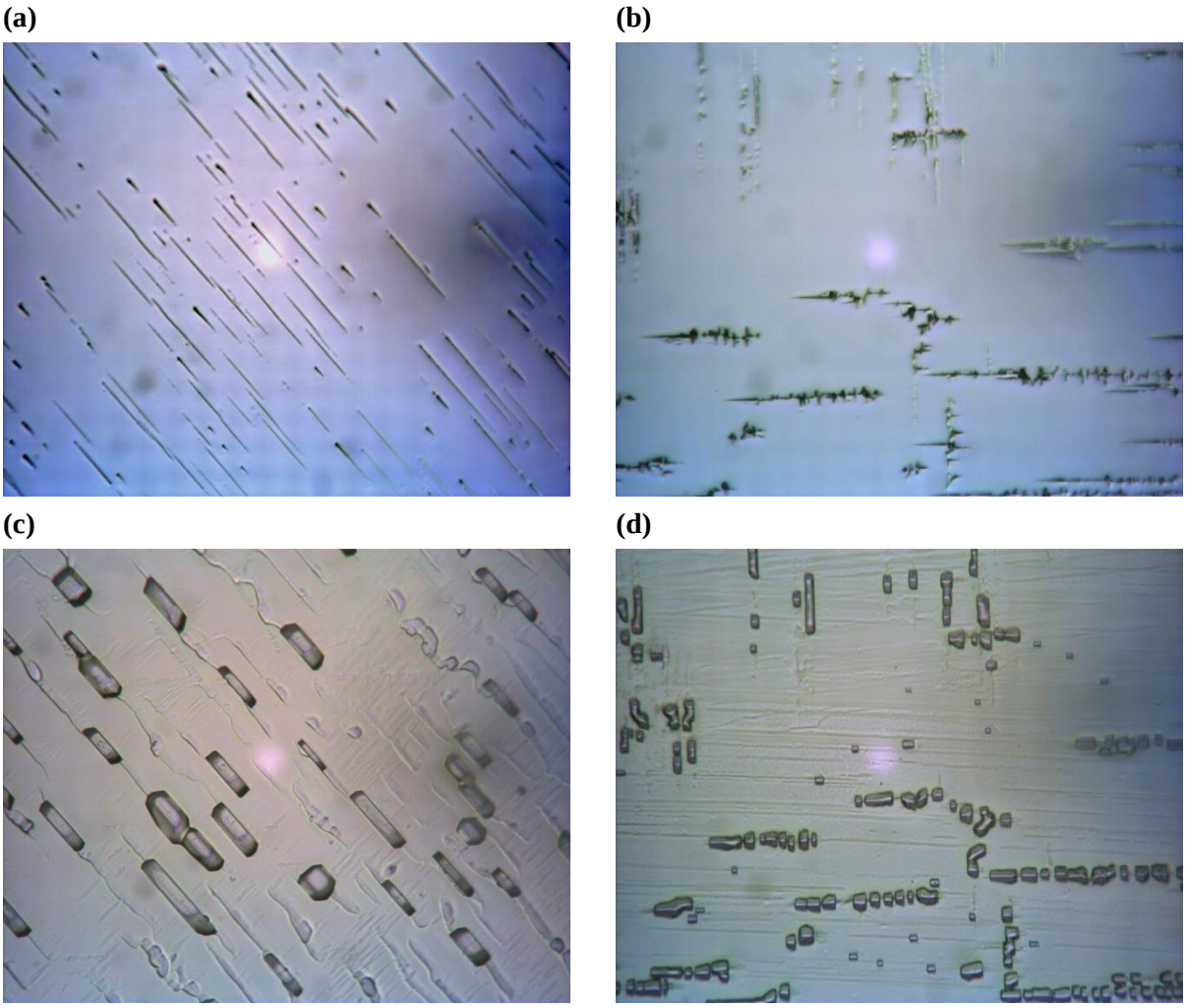

Figure 28. (a) Extended self-anneal of the primary prism face, producing "cuts" along one direction. (b) Extended self-anneal of the secondary prism face, producing "cuts" along two directions, perpendicular to one another. (c) Etch of the primary prism face after extended self-anneal. Note that the etch pits grow off of the "cuts" in the perpendicular direction of what is observed in normal etch pit growth. (d) Etch of the secondary prism face after extended-self anneal. The etch pits grow along the observed defects.

4.5.2 Construction of the Microscope

A brief overview of the optical set-up of the microscope is provided here, based on the diagram provided in Figure 29. A 532 nm continuous wave (CW) laser diode is used as the light source. The light passes through a linear polarizer, assembled as a sheet of polarizing film held between two glass plates. Two mirrors (M1 and M2) reflect the light and are included in the path as a means of scanning across the sample; as the position of M2 is adjusted using the piezo actuator connected to it (M2 is mounted on a translation stage), the location at which the laser beam hits beam splitter 1 (BS 1) to be reflected changes. A change in reflection position ultimately changes the position at which the beam is hitting the sample. The light then

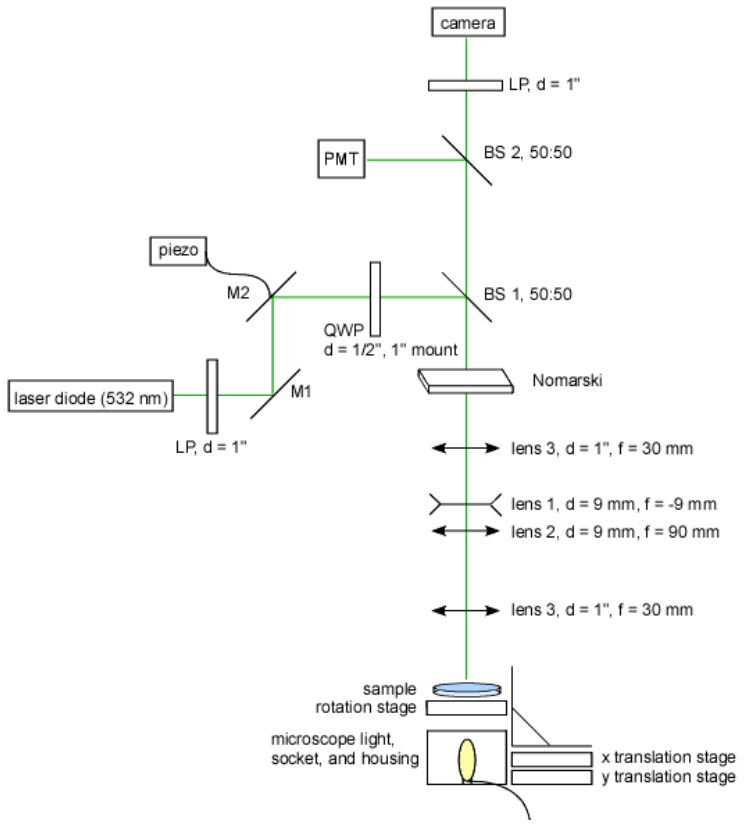

Figure 29. Optical schematic of the components of the differential interference contrast microscope.

passes through a quarter wave plate (QWP), which introduces phase retardation. By adjusting the phase of the light, the microscope image can be manipulated to have a dark or gray background when traversing flat terrain, as opposed to the white background that would normally result from the constructive interference that occurs when there is no difference in height across the surface being scanned.

At BS 1, half of the light is reflected to continue through the optics. It passes through the Nomarski prism, where it is split into two beams. The Nomarski prism specifications (Figure 30) are such that the splitting angle is 40 arc seconds and the offset distance is 10 mm at 532 nm. After the Nomarski prism, the beams are refracted to be parallel with lens 3 (f = 30 mm).

The two beams then pass through a 10:1 condenser, composed of a negative focal length lens (lens 1, f = −9 mm) and a positive focal length lens (lens 2, f = 90 mm). Lens 3 (f = 30 mm) then converges the laser beams to a single spot on the surface, which accomplishes the task of condensing the laser beam down to the smallest size possible, since light cannot be focused to a point.

The light is then reflected off of the sample and passed through the three lenses and the Nomarski prism once again to be recombined. Upon reaching BS 1, half of the light is transmitted to BS 2, where half is reflected towards the photomultiplier tube (Hamamatsu P4332), and the other half is blocked by a linear polarizer to prevent the high power light from reaching the camera. The white light that is used to image the sample passes through the same arrangement with the ultimate goal of reaching the camera to form an image.

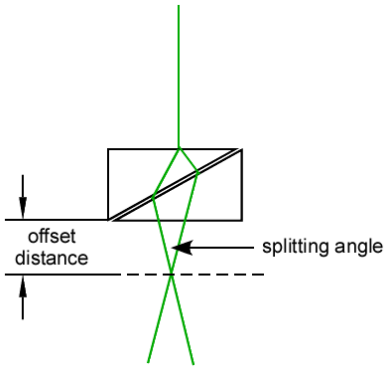

Figure 30. Definitions of the splitting angle and offset distance.

5 CONCLUSION

In spite of its ubiquity in our world, very little is truly understood about ice. Water fascinates scientists through its ability to play such a pivotal role in such a wide range of contexts. Ironically, the hydrogen bonding that allows for this flexibility and utility is also what makes it difficult to study. The molecule that is perhaps the most well-known and common in our world is also one that continues to baffle the scientists that study it.

The aim of my work has been to unravel some of these complexities and gain insight into the surface structure of ice. The surface is the key to understanding how water interacts with other molecules and also how thermodynamics play a role in shaping the behavior of water. In spite of etching having been used for over fifty years, it is clear that not everything is understood about how etch pits form and how they relate to the molecular structure of water. My hope is that this work inspires young students to enter the realm of water research and pursue further work on the differential interference contrast microscope, which I believe is the key to understanding issues such as the subtle differences in the interfacial energies of the faces of H_2O and D_2O and how growth occurs at the ice-water interface.

6 ACKNOWLEDGEMENTS

The author would like to acknowledge support from NSF Grant #CHE1306933, the Tufts University Department of Chemistry, the Tufts Summer Scholars program, and the Tufts Undergraduate Research Fund.

7 REFERENCES

(1) Spencer, N. D.; Schoonmaker, R. C.; Somorjai, G. A. Iron Single Crystals as Ammonia Synthesis Catalysts: Effect of Surface Structure on Catalyst Activity. *J. Catal.* **1982**, *74* (1), 129–135.

(2) Ritter, S. K. The Haber-Bosch Reaction: An Early Chemical Impact On Sustainability. *Chem. Eng. News* **2008**, *86* (33).

(3) Higashi, A. Growth and Perfection of Ice Crystals. *J. Cryst. Growth* **1974**, *24-25*, 102–107.

(4) Bridgman, P. W. Certain Physical Properties of Single Crystals of Tungsten, Antimony, Bismuth, Tellurium, Cadmium, Zinc, and Tin. *Proc. Am. Acad. Arts Sci.* **1925**, *60* (6), 305–383.

(5) Stockbarger, D. C. The Production of Large Single Crystals of Lithium Fluoride. *Rev. Sci. Instrum.* **1936**, *7* (3), 133–136.

(6) Talik, E. Ninetieth Anniversary of Czochralski Method. *J. Alloys Compd.* **2007**, *442* (1-2), 70–73.

(7) Pajaczkowska, A. Jan Czochralski and His Method of Crystal Growth. *Acta Phys. Pol. A* **2013**, *124* (2), 171–172.

(8) Knight, C. A. A Simple Technique for Growing Large, Optically "perfect" ice Crystals. *J. Glaciol.* **1996**, *42* (142), 585–587.

(9) Khusnatdinov, N. N.; Petrenko, V. F. Fast-Growth Technique for Ice Single Crystals. *J. Cryst. Growth* **1996**, *163*, 420–425.

(10) Bilgram, J.; Wenzl, H.; Mair, G. Perfection of Zone Refined Ice Single Crystals. *J. Cryst. Growth* **1973**, *20* (4), 319–321.

(11) Bisson, P.; Groenzin, H.; Barnett, I. L.; Shultz, M. J. High Yield, Single Crystal Ice via the Bridgman Method. *Rev. Sci. Instrum.* **2016**, *87* (3), 034103.

(12) Bisson, P. J. Hydrogen Bonding in the Prism Face of Ice Ih A Study via Sum Frequency Generation Vibrational Spectroscopy, Tufts University, 2013.

(13) Shultz, M. J.; Bisson, P. J.; Brumberg, A. Best Face Forward: Crystal-Face Competition at the Ice-Water Interface. *J. Phys. Chem. B* **2014**, *118* (28), 7972–7980.

(14) Groenzin, H. Sum-Frequency Studies of Single Crystalline Ice Ih, Tufts University, 2007.

(15) Li, I. Sum Frequency Studies of Single Crystal Ice (Ih) as Related to Its Lattice Orientation, Tufts University, 2008.

(16) Shultz, M. J.; Brumberg, A.; Bisson, P. J.; Shultz, R. Producing Desired Ice Faces. *Proc. Natl. Acad. Sci. U. S. A.* **2015**, *112* (45), E6096–E6100.

(17) Chaplin, M. Hexagonal Ice (Ice Ih) http://www1.lsbu.ac.uk/water/hexagonal_ice.html.

(18) Nelson, J. Growth Mechanisms to Explain the Primary and Secondary Habits of Snow Crystals. *Philos. Mag. A* **2001**, *81* (10), 2337–2373.

(19) Handel, R.; Davidchack, R. L.; Anwar, J.; Brukhno, A. Direct Calculation of Solid-Liquid Interfacial Free Energy for Molecular Systems: TIP4P Ice-Water Interface. *Phys. Rev. Lett.* **2008**, *100* (3), 036104–1 – 036104–4.

(20) Libbrecht, K. G. Explaining the Formation of Thin Ice Crystal Plates with Structure-Dependent Attachment Kinetics. *J. Cryst. Growth* **2003**, *258* (1-2), 168–175.

(21) Conrad, P.; Ewing, G. E.; Karlinsey, R. L.; Sadtchenko, V. Ice Nucleation on BaF2(111). *J. Chem. Phys.* **2005**,

122 (6), 064709.

(22) Bigg, E. K. The Supercooling of Water. *Proc. Phys. Soc.* **1953**, *66* (8), 688–694.

(23) Criscione, A.; Kintea, D.; Tuković, Ž.; Jakirlić, S.; Roisman, I. V.; Tropea, C. Crystallization of Supercooled Water: A Level-Set-Based Modeling of the Dendrite Tip Velocity. *Int. J. Heat Mass Transf.* **2013**, *66*, 830–837.

(24) Curie, P. On the Formation of Crystals and on the Capillary Constants of Their Different Forms. In *Crystal Form and Structure*; Schneer, C. J., Ed.; Dowden, Hutchinson & Ross: Stroudsburg, Pennsylvania, 1977; pp 41–42.

(25) Wulff, G. On the Question of the Rate of Growth and of Dissolution of Crystal Face. In *Crystal Form and Structure*; Schneer, C. J. (University of N. H., Ed.; Dowden, Hutchinson & Ross: Stroudsburg, Pennsylvania, 1977; pp 43–52.

(26) Laue, M. von. The Wulff Theorem for the Equilibrium Form of Crystals. In *Crystal Form and Structure*; Schneer, C., Ed.; Dowden, Hutchinson & Ross: Stroudsburg, Pennsylvania, 1977; pp 141–147.

(27) Libbrecht, K. G. On the Equilibrium Shape of an Ice Crystal. **2012**.

(28) Craft, Q. D.; Hook, W. A. Van. Isotope Effects in Aqueous Systems. VI. Partial Molal Enthalpies of Solution of NaCl-H2O-D2O by Freezing-Point Measurements. The Heat of Fusion of D2O. *J. Solution Chem.* **1975**, *4* (11), 923–947.

(29) Chen, B.; Ivanov, I.; Klein, M. L.; Parrinello, M. Hydrogen Bonding in Water. *Phys. Rev. Lett.* **2003**, *91* (21), 215503.

(30) Thermal Conductivity of Liquids. In *CRC Handbook of Chemistry and Physics*; 2015.

(31) Properties of Saturated Liquid D2O. In *CRC Handbook of Chemistry and Physics*; 2015.

(32) Murphy, D. B.; Davidson, M. W. Differential Interference Contrast Microscopy and Modulation Contrast Microscopy. In *Fundamentals of Light Microscopy and Electronic Imaging*; John Wiley & Sons, Inc., 2013.

(33) Brandmaier, C.; Spring, K. R.; Davidson, M. W. Reflected Light DIC Microscopy http://microscopyu.com/articles/dic/reflecteddic.html.

(34) Murphy, D. B.; Salmon, E. D.; Spring, K. R.; Abramowitz, M.; Davidson, M. W. Fundamental Concepts in DIC Microscopy http://olympus.magnet.fsu.edu/primer/techniques/dic/dicintro.html.

(35) Brice, J. C. *The Growth of Crystals from the Melt*; North-Holland Publishing Co.: Amsterdam, 1965.

(36) Rigsby, G. P. Crystal Fabric Studies on Emmons Glacier Mount Rainier, Washington. *J. Geol.* **1951**, *59* (6), 590–598.

(37) Higuchi, K. The Etching of Ice Crystals. *Acta Metall.* **1958**, *6*, 636–642.

(38) Bryant, G. W.; Mason, B. J. Etch Pits and Dislocations in Ice Crystals. *Philos. Mag.* **1960**, *5* (60), 1221–1227.

(39) Sinha, N. K. Dislocations in Ice as Revealed by Etching. *Philos. Mag.* **1977**, *36* (6), 1385–1404.

(40) Kuroiwa, D.; Hamilton, W. Studies of Ice Etching and Dislocation Etch Pits. In *Ice And Snow*; 1963; pp 34–55.

(41) Pfalzgraff, W. C.; Hulscher, R. M.; Neshyba, S. P. Scanning Electron Microscopy and Molecular Dynamics of Surfaces of Growing and Ablating Hexagonal Ice Crystals. *Atmos. Chem. Phys. Discuss.* **2010**, *10*, 2927–2935.

(42) Rosenberg, R. Why Is Ice Slippery? *Phys. Today* **2005**, *58*, 50–55.

(43) Fleur, N. St. Who Ever Said No Two Snowflakes Were Alike? http://www.nytimes.com/2016/01/23/science/who-ever-said-no-two-snowflakes-were-alike.html.